STIFFNESS OF MOUSE AORTIC ELASTIN AND ITS POSSIBLE RELATION TO AORTIC MEDIA STRUCTURE

by

Trisha Elaine Clark

B.Sc., University of Guelph, 2000
B.Ed., University of Ottawa, 2001

A THESIS SUBMITTED IN PARTIAL FULFILMENT OF
THE REQUIREMENTS FOR THE DEGREE OF

MASTER OF SCIENCE

in

THE FACULTY OF GRADUATE STUDIES

(Zoology)

THE UNIVERSITY OF BRITISH COLUMBIA
(Vancouver)

June 2013

Abstract

Aortic elastin allows arterial expansion on systole and subsequent elastic recoil during diastole, providing crucial capacitance and associated dampening of the cardiac pressure pulses. The structure and mechanical properties of the aortic wall are not uniform along its length due to the varying hemodynamic conditions to which it is exposed, but elastin's contributions to this variation are not well studied. The artery wall is a composite of two main structural proteins: elastin and collagen. Autoclaving an intact aorta removes the collagen and produces a mechanically competent vessel consisting of purified elastin, which can be used to study elastin's contribution to arterial mechanics. Although it is generally assumed that elastin's material stiffness is constant, a recent study in pigs found that it increased 30% along the thoracic aorta. I hypothesized that this increase in elastin stiffness was caused by a difference in the amount of elastin, the amount or orientation of the interlamellar elastin fibres (IEL), the partitioning of elastin between its three forms, the thickness or orientation of the elastic lamellae, or the number of elastin struts. Uniaxial tensile testing of autoclaved mouse aortas showed that elastin's stiffness is 43% lower in abdominal aortas compared with thoracic aortas, allowing the mouse aorta to be used as a model to investigate this surprising variation in elastin stiffness. Elastin structure within the thin mouse aortic walls was imaged with multiphoton laser scanning microscopy to identify any differences in the elastin structure that could cause the variation in stiffness. No difference was found between the elastin structure of the thoracic and abdominal aortas that could account for the difference in elastic modulus; however, I was not able to count the elastin struts or measure the elastin fibre packing density in the elastic lamellae and so could not reject these two hypotheses.

Preface

This dissertation is an original intellectual product of the author, T. Clark. The work was carried out under UBC Animal Care Certificate #A12-0107.

Table of Contents

List of Tables

List of Figures

List of Abbreviations

1int	artery ring cut distal to the 1st intercostal artery
6int	artery ring cut distal to the 6th intercostal artery
9int	artery ring cut distal to the 9th intercostal artery
acel	artery ring cut proximal to the celiac artery
EGTA	ethyleneglycol tetraacetic acid
IEF	interlamellar elastic fibres
ilia	artery ring cut proximal to the common iliac bifurcation
$L_{0,p}$	morphological initial length
$L_{0,m}$	mechanical initial length
$L_{0,r}$	regression initial length
lumb	artery ring cut proximal to the ilio-lumbar artery
MPLSM	multiphoton laser scanning microscopy
PBS	phosphate buffered saline
SMC	smooth muscle cells
σ_e	engineering stress
σ_l	lamellar stress

Glossary

Adventitia	The outermost layer of the artery wall (tunica adventitia).
Elastic modulus	A measure of a material's stiffness determined from the slope of a stress-strain or stress-stretch ratio curve.
Intact	The state of an aorta before autoclaving, when it contains elastin, collagen, and smooth muscle cells.
Media	The middle layer of the artery wall (tunica media).
Pre-conditioning	The initial stretching of the artery before tensile testing that ensures a consistent mechanical response.
Purified elastin	The state of an aorta after autoclaving, when it contains only elastin.
Spring constant	A measure of an object's stiffness determined from the slope of a force-displacement curve.
Strain	The displacement or stretch of an object after normalizing for the object's initial length ($\triangle L/Lo$).
Stress	The load (force / cross-sectional area) acting on and deforming an object.
Stretch ratio	The displacement or stretch of an object after normalizing for the object's initial length (L/Lo).
Volume fraction	The volume of elastin in the sample divided by the total volume of the sample.

Acknowledgements

First I would like to thank Bob Shadwick for his guidance and for being a wonderful supervisor in every respect. The positive atmosphere in the lab made me enjoy coming to school every day. I also owe a big thank you to Margo Lillie for her help throughout this whole project. She always had an open door and patiently answered my many questions. My committee members Wayne Vogl and John Gosline also provided assistance and guidance for which I am grateful.

Thank you to the Shadwick, Gosline, and Altshuler lab members for helping make the lab such a great place to work and for the many cookie runs. Thank you to Micha Ben-Zvi for starting my love-hate relationship with Matlab.

The wonderful images and second half of this thesis would not have been possible without the help of the Bioimaging Facility staff and in particular Kevin Hodgson's technical assistance with the laser beams. I would also like to thank the staff of the Animal Resource Unit who kindly took the time to help with my project.

My parents have always been there to listen and support me through several degrees and careers; without them I wouldn't be where I am today. My husband has lived with me through the trials and tribulations of this grad school adventure; thank you, Randy, for your encouragement and for always supporting all of my projects.

Introduction

William Harvey first described the circulation of the blood in 1628 (Harvey, 1628). Prior to this it was thought that blood was produced in the liver, transported to the heart via the veins, combined with “vital spirits” in the heart and delivered to the body via the arteries. It is now known that arteries are not only a conduit for blood, but also smooth the pulsatile flow of blood through the arterial system. Arteries’ expansion on systole and subsequent elastic recoil during diastole provide capacitance for the system and dampen the pressure and flow pulses from the heart’s contractions, resulting in a near constant flow of blood in the capillaries (Hales, 1733; Taylor, 1964). Stephen Hales discovered this phenomenon in 1733 and likened the arterial expansion and recoil to an air chamber on a contemporary fire engine (Hales, 1733). This air chamber analogy was popularized by Otto Frank (with the German translation *Windkessel*) and it became known as the Windkessel model. However, this model is over-simplified for a mammalian system due to complex reflections of pressure and flow waves at branch points in the arterial tree, such as the common iliac bifurcation, and interaction of the reflections with new waves from the next heartbeat (Attinger, 1964; Taylor, 1964; Fung, 1993). Fine tuning of the elasticity in the arteries affects these pressure-flow relationships and ultimately the energetic output required of the heart. For example, the pressure in the aortic arch is lower than expected because of the reflection of the pressure wave and so the pressure that the heart must work against is lower. The structure of the aortic wall is therefore not uniform along its length due to the variable pressure and flow waves to which it is exposed. This thesis used a mouse model to further investigate the finding by Lillie and Gosline (Lillie and Gosline, 2007) that the stiffness (elastic modulus) of the elastic component of the pig thoracic aortic wall increases distally along the aorta.

Components of the Artery Wall

There are three main structural components in the artery wall of vertebrates: elastic fibres, collagen, and smooth muscle. Elastic fibres are composed of elastin and glycoprotein microfibrils. Elastin, microfibrils, and collagen are all proteins produced by the smooth muscle cells. The molecules of elastin, a rubber-like protein, have a random conformation (Aaron and Gosline, 1980) and are covalently cross-linked to each other (Aaron and Gosline, 1981). Elastin has a low elastic modulus, or low stiffness, meaning that it is highly extensible when pulled with a given force. In other words, a particular stress (the force acting per cross-sectional area) produces a relatively high strain (change in length relative to the original length). In contrast, collagen has a highly ordered, triple-helical structure and a high elastic modulus, or high stiffness. The elastic modulus of elastin (1 MPa; Aaron and Gosline, 1981) is three orders of magnitude lower than that of collagen (1650 MPa; Ker, 1981). Elastic fibres will hereafter be referred to as *elastin*.

Because the artery wall is a composite of a very stiff and a very compliant material, the mechanical properties will change along the arterial tree as the proportions of these two components change. In the thoracic aorta 60% of the total protein (elastin and collagen) is elastin, compared with 30% in the abdominal aorta (Harkness et al., 1957) and 28% in the carotid artery (Fischer and Llaurado, 1966). Therefore the elastic modulus (stiffness) of the arterial wall increases with increasing distance from the heart (by 1.5 times in the abdominal aorta compared with the thoracic at 100 mm Hg; Harkness et al., 1957; Bergel, 1960; Fischer and Llaurado, 1966). The lower elastic modulus of the thoracic aorta allows it to expand on systole, thereby providing capacitance to the system by way of a reservoir of blood to be delivered during diastole.

Structure of the Artery Wall

The arterial wall of mammals is composed of three layers (see Figure 1). The innermost layer, the tunica intima, is made up of endothelial cells. The outermost layer, the tunica

adventitia, contains mainly collagen. This thesis will focus on the middle layer, the tunica media, which contains elastin, smooth muscle cells and collagen (Fung, 1993).

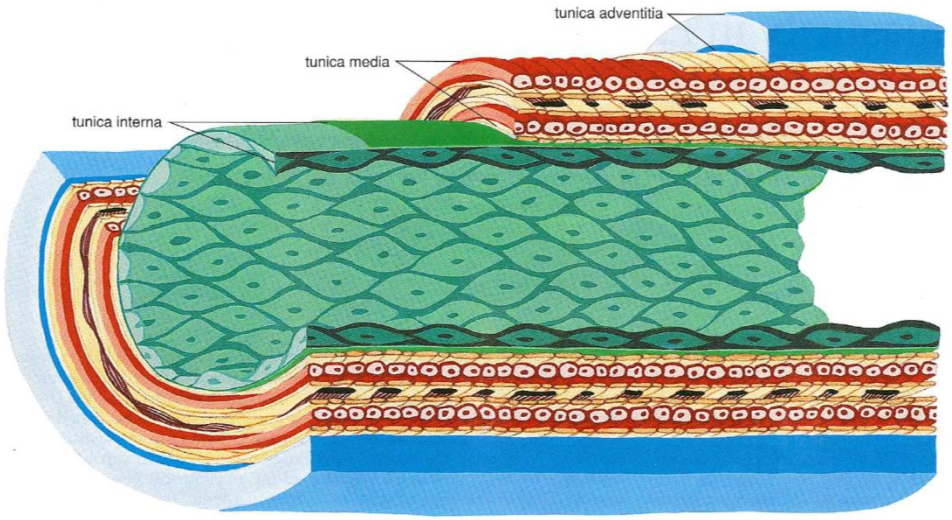

Figure 1. The structural regions of the arterial wall: tunica intima (endothelial cells), tunica media (collagen, elastin, smooth muscle), and tunica adventitia (mainly collagen).(Shadwick, 1998) Reprinted with permission.

The tunica media (media) has a complex structure and many authors have described it, with some conflicting results (Clark and Glagov, 1985; Davis, 1993; Dingemans et al., 2000; O'Connell et al., 2008; Wolinsky and Glagov, 1964; Wolinsky and Glagov, 1967). It is made up of lamellar units which are repeating units of elastin, collagen, and smooth muscle (see Figure 2). The lamellar unit is the structural and functional unit of the aortic media but its exact structure has seen some debate (Clark and Glagov, 1985; Davis, 1993; Wolinsky and Glagov, 1967). In all mammalian species, the lamellar units are on average 15 μm thick (6 μm thick in the mouse) at mean physiological pressure and the number of lamellar units is proportional to the radius of the aorta, thus larger animals have more lamellar units but the structure of the unit itself is believed to be the same (Wolinsky and Glagov, 1967).

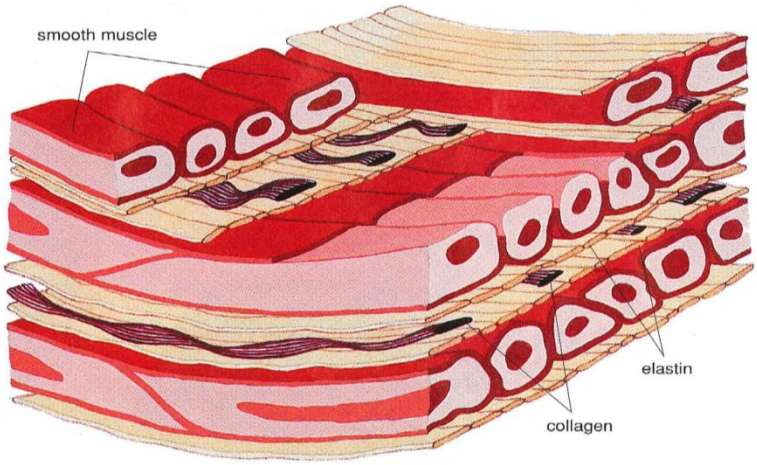

Figure 2. A section of tunica media showing the repeating lamellar units of elastin, collagen, and smooth muscle. (Shadwick, 1998) Adapted from (Clark and Glagov, 1985). Reprinted with permission.

The structure of the lamellar unit generally consists of layered sheets of elastic lamella fibres with collagen and smooth muscle cells in between. The elastin, collagen and smooth muscle cells are oriented mainly circumferentially. Elastin is present in the form of elastic lamellar sheets, interlamellar elastin fibres, and, in rat abdominal aortas, radial struts in the proportions of 70%, 27%, and 2% by volume respectively (O'Connell et al., 2008). As noted by O'Connell (2008), struts can also be seen in SEM images of aortae in sheep, rabbit, dog, and cat from a study by Song and Roach (Song and Roach, 1985).

The lamellar sheets (elastic lamellae) are composed of thick elastin fibres oriented largely circumferentially. The interlamellar elastin fibres (IEF) are thin and protrude obliquely from the elastic lamellae in radial and circumferential orientations (Davis, 1993; O'Connell et al., 2008). In mouse and rat thoracic aortas the IEF extend from the elastic lamellae to the surface of the smooth muscle cells. Inside the smooth muscle cells the contractile filaments are aligned in the same oblique direction as the IEF, forming a continuous line through the cell to the other side where another IEF extends to the adjacent lamella. This connection forms a *contractile-elastic unit*, possibly allowing tensions to spread from one elastic lamella to the next (Davis, 1993; O'Connell et al., 2008). A study of human thoracic aortas did see extensions of the smooth muscle cells in contact with *protrusions* or *streaks* of the elastic lamella (possibly IEF),

but most of the interlamellar elastin was described as a network of elastin that had few connections to the elastic lamellae (Dingemans et al., 2000). The radial elastin struts are thick and project radially from one elastic lamella to the next. The smooth muscle cells between elastic lamellae are oriented circumferentially with a radial tilt and are surrounded on all sides by elastin: elastic lamellae next to their luminal and adventitial surfaces, radial struts on one side and IEF on the other. Collagen fibres are oriented circumferentially in parallel layers in close proximity to the smooth muscle cells (O'Connell et al., 2008).

Function of the Artery Wall

The artery wall functions as a composite or two-phase material (Roach and Burton, 1957; Wolinsky and Glagov, 1964). Figure 3 shows a typical stress-strain curve for an artery: as a force is applied over the cross-sectional area of the sample, the sample changes in length. As seen on the graph, the change in length is not proportional to the force applied. Roach and Burton (Roach and Burton, 1957) showed that this J-shaped stress-strain curve is due to the combined properties of the elastin and collagen. In the lower portion of the graph (low strain), the slope or elastic modulus is lower meaning the artery is less stiff; this is due to the contribution of elastin. In the upper portion of the graph (high strain), the slope or elastic modulus is higher meaning the artery is stiffer; this is due to the contribution of collagen. In this way the artery is able to expand but not rupture.

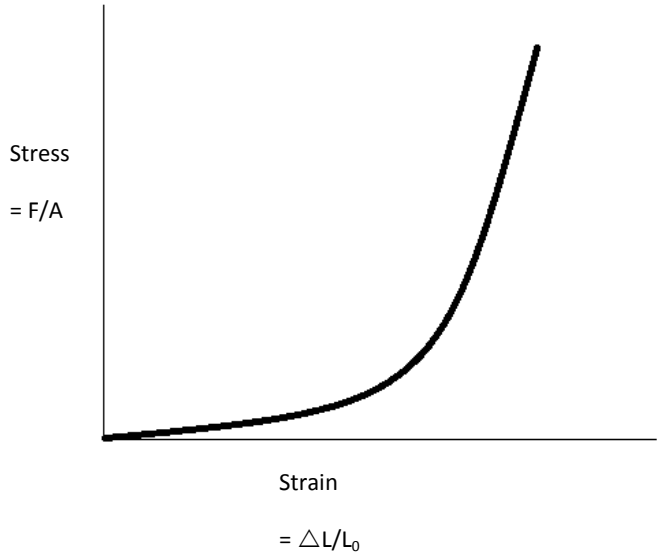

Figure 3. Typical stress-strain curve of an artery. F, force; A, cross-sectional area; △L, change in length; L_0, original length.

Wolinsky and Glagov proposed that the collagen fibres withstand most of the load at physiological pressures while the elastin distributes the load evenly throughout the artery wall (Wolinsky and Glagov, 1964). However, other authors proposed that both elastin and collagen withstand significant amounts of the load at physiological pressures (Dobrin and Canfield, 1977; Shadwick, 1999). Recently, Lillie et al. (Lillie et al., 2012) determined that in pig thoracic aortas collagen is recruited at systolic stretches in the proximal thoracic and below diastolic stretches in the distal thoracic. The structural arrangement that allows for this recruitment is not known.

Longitudinal Strain

Arteries are under a longitudinal strain *in vivo* and recoil when they are excised. The amount of longitudinal displacement is often reported as a longitudinal stretch ratio of x/x_0, where x and x_0 are the *in vivo* and unloaded, excised lengths respectively. In the mouse, the longitudinal stretch ratio varies by region, from 1.1 in the ascending aorta to 1.6 at the common iliac bifurcation (Guo and Kassab, 2003).

Purified Elastin Aortic Stiffness

Elastin and glycoprotein microfibrils are insoluble and resistant to degradation. It is therefore possible to obtain an aorta consisting only of elastic fibres (termed purified elastin) through degradation of the other components of the arterial wall. This degradation can be accomplished by autoclaving the aorta at a high temperature and pressure (121 ^{o}C, 101 kPa; Partridge et al., 1955; Lillie et al., 1994; Lillie et al., 1998; Gundiah et al., 2007), conditions under which the collagen is denatured and solubilized but the elastin is not because it is stabilized by permanent covalent crosslinks.

Lillie and Gosline (Lillie and Gosline, 2007) investigated the mechanical properties of purified elastin rings from pig thoracic aorta and found, surprisingly, that the circumferential elastic modulus increased with increasing distance from the heart (longitudinal position). The same trend was found in bovine thoracic aorta (Zou and Zhang, 2009). The elastic modulus of an intact (non-autoclaved) aorta also increases with increasing longitudinal position, but presumably this is due to the relative increase in collagen proportion. In a purified elastin ring where only elastin is present, the difference in elastic modulus may be due to the morphology of the elastin; for example, relatively more fibres in the distal thoracic aorta oriented circumferentially versus longitudinally than in the proximal aorta (Lillie and Gosline, 2007). This thesis investigated the mechanistic basis for the increase in elastic modulus with longitudinal position using the mouse as a model because of its small size (which is important when using multiphoton laser scanning microscopy, as will be explained later). The first step in this study was therefore to verify that the mouse was a suitable model by determining if the elastic modulus of a purified elastin mouse aorta also changes with increasing longitudinal position.

Microscopy Technique

This thesis used multiphoton laser scanning microscopy (MPLSM) to investigate the structure of the mouse aorta wall with the aim of explaining any changes in elastic modulus along the purified elastin mouse aorta.

A multiphoton laser scanning microscope (MPLSM) uses a laser to scan a thin plane of tissue and excite the molecules in that tissue. The laser sends out very short (150 femtosecond) pulses of light so that two photons of light (from subsequent pulses) interact with a molecule of the tissue and their combined energy causes an excitation. If the tissue is fluorescent or has been linked with a fluorescent molecule, the excitation causes it to fluoresce. Since the two photons interact on only one plane, any emitted fluorescent light must have come from the plane of interest and is therefore in-focus light from the object of interest. MPLSM is thus carried out in a darkened environment and all emitted light is collected and processed into a digital image of the tissue sample (Zipfel et al., 2003).

Elastin autofluoresces so no marker is needed when using this technique. Collagen doesn't autofluoresce, but when two photons interact with its surface structure light is emitted at half the excitation wavelength. This is called second harmonic generation (SHG). The light from SHG can be collected separately. The light from both sources is then processed to create one three-dimensional image of both elastin and collagen (Zipfel et al., 2003).

The use of MPLSM in this thesis had several advantages. (1) MPLSM does not affect the structural integrity of the arterial wall (Megens et al., 2007). (2) MPLSM doesn't require the tissue to be fixed or dyed prior to imaging, thereby avoiding any potential artefacts. (3) The mouse aortic wall is sufficiently thin that it could be imaged in its entirety with minimal scattering or absorption of light before collection, thereby producing a clear image.

Mouse Model

The mouse is a useful model for diseased and healthy aortic function in other mammalian taxa. The small size of the mouse aorta (four to six elastic lamellae in the media; approximately 100 μm aortic wall thickness in no-load state) allowed the entire thickness of the wall to be imaged using MPLSM.

Thesis Objectives and Hypotheses

Many questions remain about the basic structure and function of artery walls. For example:

- How are the elastic lamellar sheets, interlamellar elastin fibres, and smooth muscle cells connected?
- Are elastin and collagen linked mechanically in series or parallel?
- How is load transferred from elastin to collagen and at what pressure does this take place?

The purpose of my thesis was to add to the understanding of the basic structure and function of arteries, which is necessary to formulate models of arterial function for bioengineering or disease states. Lillie and Gosline (Lillie and Gosline, 2007) showed that the elastic modulus of pig purified elastin thoracic aorta increases with longitudinal position; this thesis investigated how the elastic modulus changes. I used the mouse as a model for this investigation so first had to verify its suitability by determining if the elastic modulus of purified elastin aorta increases with longitudinal position in the mouse as it does in the pig. The specific objectives of my thesis were to:

1) Determine if the elastic modulus of elastin in the intact and purified elastin mouse aorta changes with longitudinal position.
    - My prediction was that the elastin in the mouse aorta would become stiffer with increasing distance from the heart. This was found to be true of pig thoracic aortas and mouse and pig aortas are similar in other aspects of structure and function.
2) Identify, using multiphoton laser scanning microscopy, differences in the structural organization of elastin between the proximal and distal aorta that might contribute to the

difference in elastic modulus. There are five hypotheses for what could be changing in the elastin 3D structure along the aorta: (1) The amount of elastin. (2) The amount of interlamellar elastin fibres (IEF) or their orientation. (3) The partitioning of elastin between its three forms (elastic lamellae, IEF, and struts). (4) The elastic lamellae thickness or orientation. (5) The number of elastin struts. A sixth hypothesis, which is not tested in this study, is that the cross-linking density of the elastin protein itself could change along the aorta.

Materials and Methods

Two types of experiments were performed: Uniaxial tensile tests to study the mechanical response of intact and purified elastin aortas and microscopy to determine the elastin 3D morphology within an intact aorta.

Experimental Animals

For the mechanical testing, female, sexually mature Balb/c mice (n = 9, aged 105 ± 56 d, weight 23.3 ± 1.9 g) were obtained from the University of British Columbia Animal Care Centre. For the morphology, female, sexually mature Balb/c mice (n = 8, aged 104 ± 44 d, weight 22.0 ± 1.5 g) were obtained from Charles River and housed at the University of British Columbia Animal Resource Unit. The animals were euthanized by an Animal Resource Unit technician according to UBC Animal Care approved protocol and dissections were started as soon as possible (within one hour of death).

Mechanical Testing

Experimental Protocols

Transverse rings were cut from mouse thoracic and abdominal aortas and stretched uniaxially in the circumferential orientation to determine their elastic modulus. The rings were then autoclaved to remove the collagen and smooth muscle cells, and retested.

Ring Preparation

The aorta was carefully excised from the aortic arch to the common iliac bifurcation. Loosely adhering tissue was carefully removed with fine forceps. Rings approximately 1 mm wide were cut from the aorta with a fresh razor blade at six locations (see Figure 4), three in the thoracic aorta: distal to the 1st intercostal artery (*1int*), 6th intercostal artery (*6int*), and 9th intercostal artery (*9int*), and three in the abdominal aorta: proximal to the celiac artery (*acel*), ilio-lumbar artery (*lumb*), and common iliac bifurcation (*ilia*).

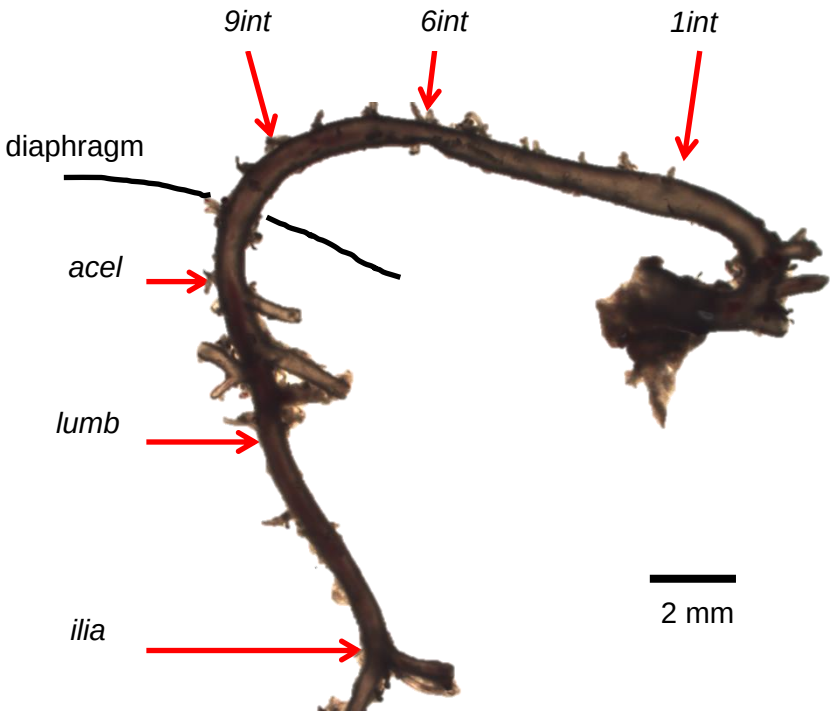

Figure 4. Image of a mouse aorta from the aortic arch (top right) to the common iliac bifurcation (bottom middle). A black line indicates the location of the diaphragm. Red arrows indicate where six rings were cut from the aorta. Three rings were from the thoracic aorta: *1int*, *6int*, and *9int* (distal to the first, sixth, and ninth intercostal artery respectively) and three from the abdominal aorta: *acel*, *lumb*, and *ilia* (proximal to the celiac artery, ilio-lumbar artery, and common iliac bifurcation respectively). The curvature is natural.

Photos of the rings in phosphate buffered saline (PBS) solution were taken using a Nikon SMZ800 dissecting microscope and QImaging MicroPublisher 3.3 RTV camera (2048 x 1536 pixel resolution) with QCapture 2.70.0 software to determine wall thickness, width and initial length. The PBS solution had the following composition (in mM): 136.9 NaCl, 2.7 KCl, 6.1 Na_2HPO_4, and 1.0 KH_2PO_4.

Prior to testing, the intact rings were soaked in PBS and ethyleneglycol tetraacetic acid (EGTA) solution for 10 minutes to inactivate the smooth muscle cells in the vessel wall (Cox, 1983). The PBS and EGTA solution had the following composition (in mM): 136.9 NaCl, 2.7 KCl, 7.5 Na_2HPO_4, 1.0 KH_2PO_4, and 2.0 EGTA.

The smooth muscle cells are destroyed during autoclaving so this step was not necessary for purified elastin rings.

Mechanical Testing Setup

Individual rings were mounted on one of two sets of hooks depending on their size. Because of the large difference in diameter between the thoracic and abdominal rings, the same size of hook could not be used for all rings (the larger hooks would not fit in the smaller rings and the smaller hooks cut into the larger rings during testing). *1int*, *6int*, *9int* and *acel* rings were mounted on hooks made from 30-gauge syringe needles with an outer diameter of 0.35 mm. *Ilia* and *lumb* rings were mounted on hooks made from acupuncture needles with an outer diameter of 0.12 mm. The ring sample was placed over the two hooks, as close as possible to the vertical portion of the hook without interfering with it (see Figure 5). The compliance of the hooks was measured and accounted for in the data analysis.

Testing was done at room temperature (21 ºC) in a PBS and EGTA bath for intact rings or a PBS bath for purified elastin rings. The upper hook was attached to a 0.1 N load cell and hydraulic actuator.

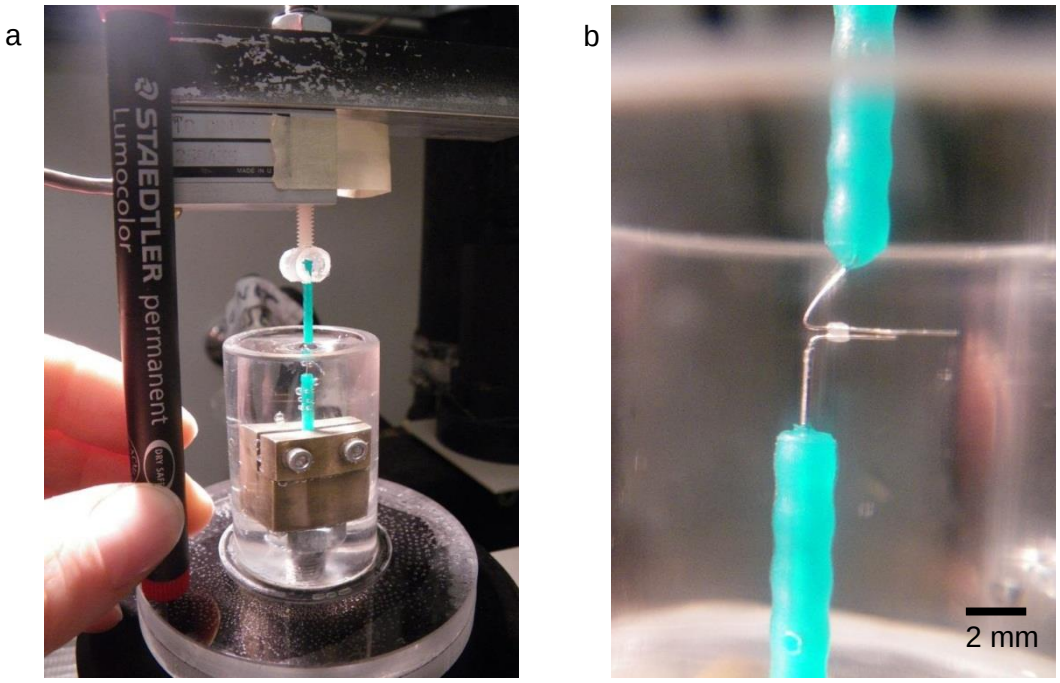

Figure 5. Uniaxial tensile testing setup with the MTS 858 Mini Bionix.(a) Setup showing hooks in PBS bath and 0.1 N load cell. Staedtler permanent marker is shown for scale. (b) Close-up view showing both hooks through an abdominal aorta ring.

Mechanical Testing

Uniaxial tensile testing was performed using an MTS 858 Mini Bionix (see Figure 5) and data were recorded with Teststar IIs Station Manager Version 3.5C 1817 software. Testing was performed under displacement control at 1 Hz in a sinusoidal cycle that was set for a maximum displacement. The tissues were pre-conditioned until a consistent mechanical response was obtained. The testing routines were identical for all rings.

For intact rings (see Table 1), the maximum displacement was set so each ring would be stretched to similar stretch ratio (approximately 1.5). Displacements were 0.8 mm for *1int*, *6int* and *9int* rings (thoracic), 0.6 mm for *acel* rings (abdominal), and 0.4 mm for *lumb* and *ilia* rings (abdominal). The intact rings were pre-conditioned for 20 cycles. Following pre-conditioning, the initial displacement (distance between hooks) was re-set to take up any slack in the ring, and then the ring was tested for 20 cycles.

Ring Location	Ring State	Pre-conditioning 1		Pre-conditioning 2		Testing	
		Maximum displacement (mm)	# cycles	Maximum displacement (mm)	# cycles	Maximum displacement (mm)	# cycles
1int, *6int*, *9int*	intact	0.8	20	N/A	N/A	0.8	20
acel	intact	0.6	20	N/A	N/A	0.6	20
lumb, *ilia*	intact	0.4	20	N/A	N/A	0.4	20
1int, *6int*, *9int*, *acel*	purified elastin	0.4	5	0.2	5	0.4	20
lumb, *ilia*	purified elastin	0.4	5	N/A	N/A	0.4	20

Table 1. Maximum displacement and number of sinusoidal cycles used during tensile testing for pre-conditioning and testing of mouse aorta rings.

The purified elastin rings broke easily during testing so a smaller maximum displacement and second pre-conditioning were used (see Table 1). For *1int*, *6int*, *9int* and *acel* rings, the maximum displacement was set to 0.4 mm for five pre-conditioning cycles. The initial displacement distance was then re-set and the maximum displacement was set to 0.2 mm for an additional five pre-conditioning cycles. This procedure was determined through trial and error to result in few broken rings. For the testing cycles, the initial displacement distance was again re-set and the maximum displacement was set to 0.4 mm for 20 cycles. For *lumb* and *ilia* rings, the maximum displacement was set to 0.4 mm throughout. The rings were pre-conditioned for 5 cycles, the initial displacement distance was re-set and the rings were tested for 20 cycles.

Measuring Hook and Transducer Compliance

The tensile tester was used to determine the compliance of the hooks and the force transducer itself. Both hooks were placed through a hole in the centre of a piece of steel then the tensile tester was displaced by 0.02 mm and the corresponding force was recorded (see Figure 6). The stiffness of steel is much greater than that of the hooks and transducer so any displacement in this system would come from the bending of the hooks and/or transducer. This procedure was repeated with both sets of hooks used for both the thoracic and abdominal ring testing.

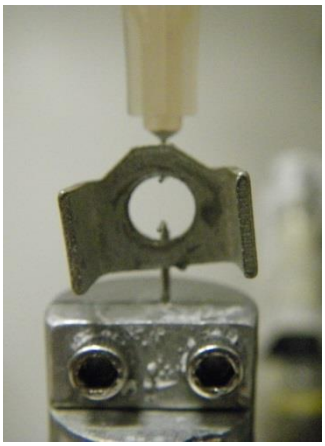

Figure 6. Setup used to test the compliance of the hooks and force transducer. The hooks were put through a hole in a piece of steel then the tensile tester was displaced 0.02 mm.

Autoclaving

After tensile testing the intact rings were autoclaved at 121 ºC using a Steris Amsco Lab 250 Laboratory Steam Sterilizer. To find the optimal autoclaving time that would remove the collagen and smooth muscle from the aorta wall but not affect the elastin (which is much more robust than collagen), rings were autoclaved and tensile testing redone for several autoclave durations (see Table 2). The rings were split into three batches to test the various autoclave times so that each ring was only tested three or four times. This was necessary because re-testing can physically degrade the tissue. Also, the autoclave time does not include the warm-up or cool-down times that are necessary for every round of autoclaving. Minimizing the rounds of autoclaving minimizes this extra time.

Sample Size	Cumulative Autoclave Time (h)		
	1st round	2nd round	3rd round
1	1	2	4
5	2	4	N/A
3	4	8	N/A

Table 2. Cumulative autoclave times for mouse aorta rings. Rings underwent mechanical testing after each round of autoclaving.

Data Analysis

Determining Ring Dimensions

Photos taken of the rings in PBS solution were analyzed using ImageJ software (National Institutes of Health) to determine the width of the rings (see Figure 7 a and c). A thin (approximately 0.2 mm) cross-section was then sliced off with a razor blade and a photo taken in PBS solution to determine the wall thickness (see Figure 7 a and d).

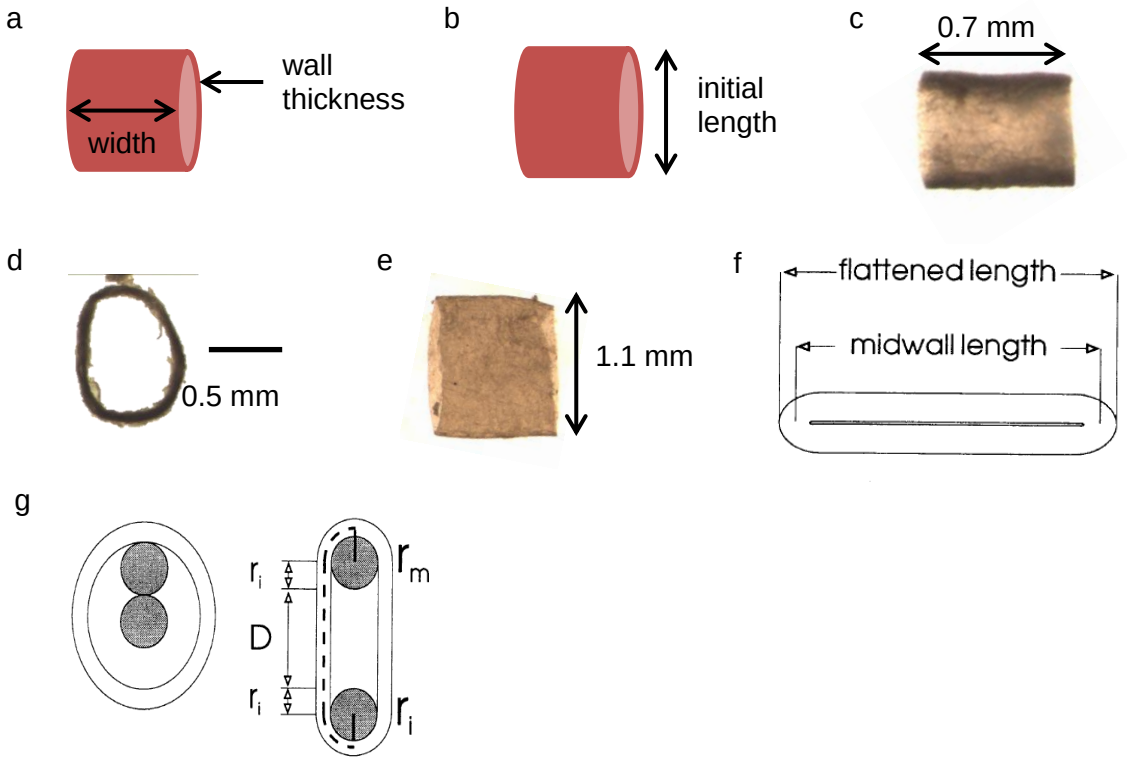

Figure 7. Schematics showing ring dimensions: width and wall thickness (a), and initial length (b). Photos of rings in PBS solution were used to determine ring width (c), wall thickness (d) and initial morphological length (e). (f) Initial morphological length ($L_{0,p}$) calculated using the flattened length of the tissue. (g) Initial mechanical length ($L_{0,m}$) calculated using the tensile testing machine when the sides of the ring are just parallel but before further stretching. r_m = midwall radius, r_i = hook radius, D = distance between the hooks (Lillie et al., 1994).

Due to the difficulty of accurately measuring the initial length of the rings (L_0), three methods described by Lillie (Lillie et al., 1994) were compared.

Morphological length: the initial length ($L_{0,p}$) was determined by placing the ring in PBS solution on a glass slide, putting a cover slip over it, and drawing out the solution with a tissue until the ring was just lying flat (see Figure 7 e and f). A photo was then taken and the length

measured using ImageJ software. The wall thickness was used to calculate the midwall length (see Figure 7 f).

Mechanical length: the initial length was calculated using the length at which the sides of the ring became parallel when mounted on the tensile testing machine (see Figure 7 g), as determined by sight (with a magnifying glass) prior to testing. This represents the length at which the ring has been deformed from a cylindrical orientation but before any further stretching. The initial mechanical length ($L_{0,m}$) is calculated as

$$L_{0,\mathrm{m}} = \pi r_m + 2r_i + D \quad (1)$$

where r_m is the midwall radius, r_i is the hook radius and D is the distance between the hooks (Lillie et al., 1994).

Regression length: the initial length ($L_{0,r}$) was determined by plotting the force exerted against the length of the ring during tensile testing (see Figure 8). The length was calculated as in Equation 1 except displacement of the tensile tester was used in place of D. A line was drawn through the initial part of the curve where there is no increase in force and another line drawn through the curve where it has a constant slope. The point of intersection of these two lines was taken to be the length at which the force is zero, in other words, the initial length. Note that the force is greater than zero at the initial length because of the force required to deform the ring from a cylindrical shape.

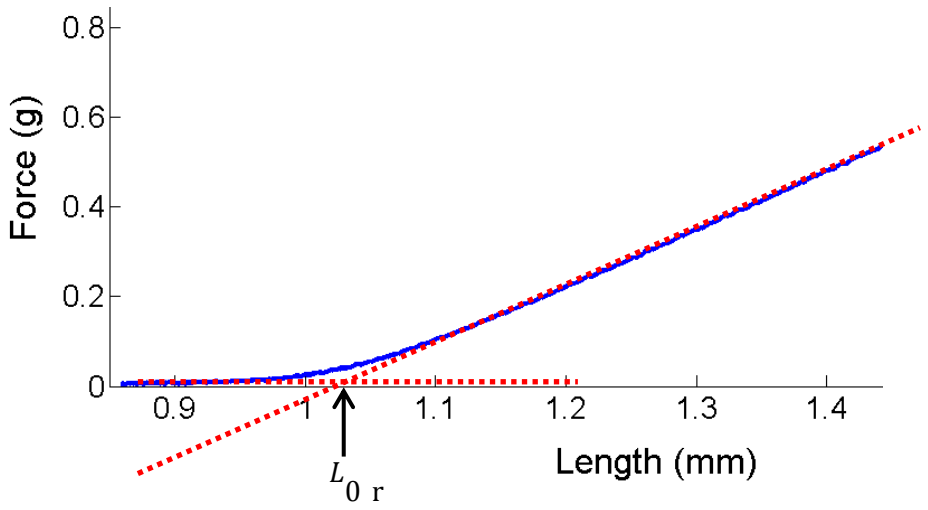

Figure 8. Curve showing how regression initial length was calculated using data from the tensile tests. Red dotted lines show where curve is zero and constant slope. The point of intersection of these lines is the initial length ($L_{0,r}$).

Hook and Transducer Compliance

The spring constant (stiffness) of the hooks and force transducer was calculated by taking the slope of the force-displacement curve for tests with the rigid steel link. The stiffness of the 30 gauge needle system and acupuncture needle system was 1.50 N/mm and 0.52 N/mm respectively. The displacement (d) that was due to compliance of the hooks and transducer was calculated as

$$\mathrm{d} = \frac{F}{hook\ \&\ transducer\ stiffness} \tag{2}$$

where *F* is the force. This correction factor, d (0.002 mm at a force of 3 mN, for example), was then subtracted from the displacement as recorded by the tensile tester to give the displacement corrected for the system compliance.

Mechanical Testing

Matlab code was written to analyze the uniaxial tensile testing data. Raw force data and displacement data (corrected for hook and transducer compliance) from each ring test was averaged then smoothed. Each testing protocol consisted of 20 cycles; cycles 2 through 19

were averaged; the first and last cycles were discarded. A 5-point running average was then used to smooth the data.

Two methods were used to calculate stress. Engineering stress (σ_e) was calculated as

$$\sigma_e = \frac{F}{A} = \frac{F}{2 \times w \times h} \quad (3)$$

where *F* is the force on the ring, *A* is the cross-sectional area of that ring after autoclaving (purified elastin ring), *w* is the undeformed width and *h* is the undeformed wall thickness. The purified elastin cross-sectional area was used to normalize the forces of both the intact and purified elastin rings. Since the adventitia had been removed during autoclaving, this area is that of only the media. The cross-sectional area used in Equation 3 includes not only the elastin that is resisting the stretch but also the spaces between elastic lamellae. To account for this and exclude the spaces, lamellar stress (σ_l) was calculated as

$$\sigma_l = \frac{F}{2 \times w \times number\ of\ elastic\ lamellae \times average\ thickness\ of\ lamellae} \quad (4)$$

MPLSM was used to determine the number and average thickness of elastic lamellae at the *6int* and *ilia* ring locations (see MPLSM Images pg. 25). These values were used to normalize the respective rings.

Stretch ratio (λ) was calculated as the length of the loaded ring divided by the initial length (L_0) of that ring after autoclaving. The purified elastin initial length was used for both the intact and purified elastin rings.

The elastic modulus (E) was taken as the slope of the stress-stretch ratio curve at a low stretch where the slope is constant (see Figure 9). This represents the area where elastin is primarily resisting the stretch. This region of the curve was determined individually by looking at the curve for each ring and was in the range of 1.1 – 1.25 stretch ratio.

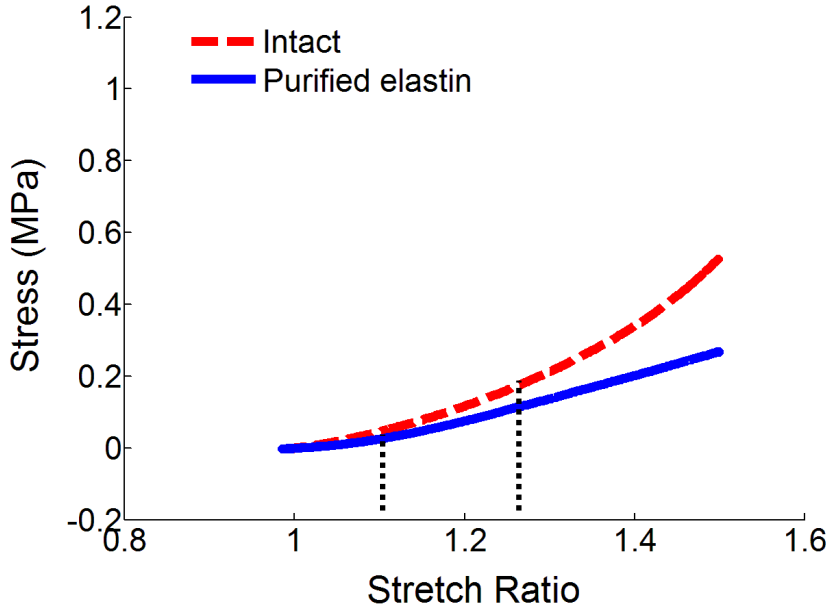

Figure 9. Stress-stretch ratio curves showing range for modulus calculation for an intact (red) and purified elastin (blue) abdominal ring (*ilia* position). The slopes of the curves between the two black dotted lines are the elastic moduli.

Statistical Analysis

Data are reported as means ± 95% confidence intervals.

A two-way ANOVA followed by a multiple comparison test (using Matlab software) was used for the statistical analysis of the elastic moduli at the six positions along the aorta. Data were missing for some positions due to broken rings, so two mice were excluded from the statistical analysis (having two broken rings each). One mouse had one broken ring so the mean modulus at that position was used to replace that missing value. As such, a sample size of seven was used for the analysis. Statistical significance was assumed at $P<0.05$.

Multiple linear regression (using Matlab software) was used to determine whether age or weight of the mouse had an effect on elastic modulus. If the 95% confidence interval of the slope of the regression included zero there was no effect.

Morphology

Experimental Protocol – Histology

Histological tissues samples were obtained for one female Balb/c mouse (aged 186 d; from Charles River). Immediately after death the aorta was infused in situ with a fixative solution (1.5% glutaraldehyde and 1.5% formaldehyde) at approximately physiological pressure. The aorta was then excised and tissue sections (5 μm thick) prepared using Van Gieson's stain.

Experimental Protocols – Multiphoton Laser Scanning Microscopy

The aortas of euthanized mice were filled with agarose gel under pressure to maintain physiological stretch, then excised. The thoracic and abdominal aortas were then imaged using MPLSM.

Sample Preparation

The aorta of the euthanized mouse was exposed in the body cavity and the vena cava was severed. A needle was inserted into the left ventricle and warm (approximately 37 ºC) PBS solution was infused through the aorta to clear it of blood. Warm agarose (1.5% in PBS solution, gel temperature 36 – 42 ºC, gel strength >1000 g/cm^2) was then injected into the aorta via the left ventricle. The agarose gels upon cooling, thereby maintaining the physiological stretch in the aorta. The aim was to keep the aorta filled to a pressure of 10 – 16 kPa (75 – 120 mmHg). A pressure transducer was used to monitor the aortic pressure while the agarose was being injected, but once the agarose solidified the pressure could not be confirmed. The aorta was ligated at the aortic arch, the subclavian arteries, the left renal artery, and distal to the common iliac bifurcation. The aorta was then excised and photos were taken in PBS solution (see Figure 10 a and b, and Stretch Ratios below). Adventitial collagen was then carefully removed by dissection from a section of the abdominal aorta. This step was necessary to allow the laser of the MPLSM to penetrate through the thick adventitia in order to image the elastin below. The thoracic and abdominal aortas were mounted separately, ventral side up, in a chamber filled with PBS solution.

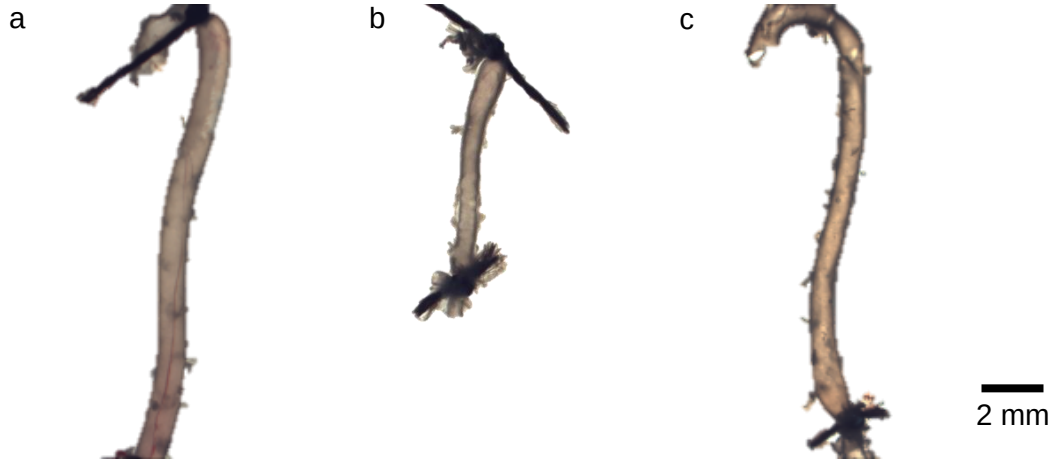

Figure 10. Images of aortas with and without agarose gel. Thoracic (a) and abdominal (b) aortas after being injected with agarose and excised.(c) The same thoracic aorta as in (a) after agarose gel was removed. Photos taken in PBS solution.

Stretch Ratios

To determine the circumferential and longitudinal stretch ratios of the aortas after agarose injection, photos of the aortas were taken (using a Nikon SMZ800 dissecting microscope and QImaging MicroPublisher 3.3 RTV camera with QCapture 2.70.0 software) when full of agarose prior to MPLSM. After MPLSM, one of the ligatures was removed and the agarose gel was carefully squeezed out of the aorta with fine forceps in a PBS solution and another photo was taken (see Figure 10). Image J was then used (as above) to measure the diameter of the aorta and the stretch ratios were calculated.

To relate the circumferential stretch ratio to the corresponding physiological pressure in the aorta, a test inflation with PBS solution was done on one female Balb/c mouse (weight 26.0 g, age 186 d). The aorta was exposed in the body cavity and photos were taken at 0 kPa (see Figure 11). PBS solution was then injected into the aorta via a cannula in the aortic arch while the pressure was recorded with a pressure transducer. When the mean physiological pressure of 14 kPa (105 mm Hg) was reached, photos were taken. All photos were taken with the dissecting microscope and camera as above. Image J was then used to measure the diameter and the circumferential stretch ratio was calculated.

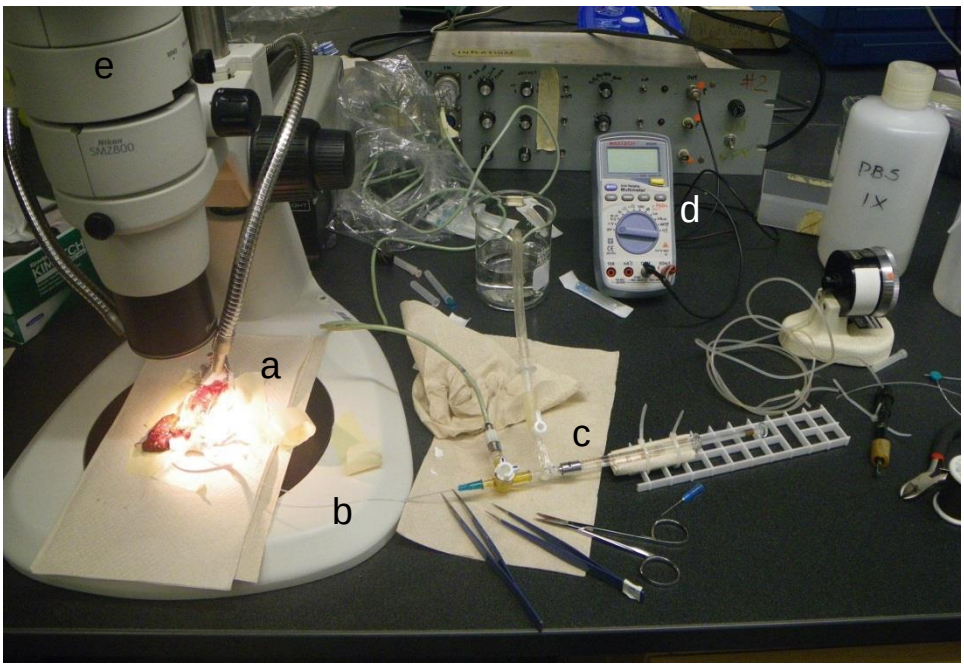

Figure 11. Experimental setup used to determine the circumferential stretch ratio at physiological pressure in a euthanized mouse. (a) mouse; (b) catheter; (c) syringe with PBS solution; (d) pressure transducer; (e) dissecting microscope with camera.

Multiphoton Laser Scanning Microscopy

The aortas were imaged at one location in each of the thoracic and abdominal aortas. Thoracic images were taken close to the 6th intercostal artery (*6int* ring location, see Figure 4) and abdominal images just proximal to the common iliac bifurcation (*ilia* ring location, see Figure 4). Images were obtained with an Olympus FV1000 multiphoton laser scanning microscope, 25X objective with numerical aperture of 1.05, and SpectroPhysics Mai Tai HP laser with DeepSee dispersion compensation unit and Fluoview version 3.1 software using an 800 or 810 nm excitation wavelength. A 485 nm long-pass filter was used followed by a 405/30 nm filter to collect the second harmonic generation signal from collagen. A 495-540 nm band-pass filter was used to collect the signal from the elastin autofluorescence. The pixel dwell time was 4 µs at an average laser power of 22 mW. The laser intensity was adjusted for depth during the scan (higher intensity at deeper depths into the tissue). The image scan size was 170 µm x 170 µm at 0.165 µm/pix. Successive scans were done such that images were obtained for the entire thickness of the aorta wall.

Data Analysis

Histology

A Zeiss Axio Scope.A1 microscope with AxioCam MRc camera (1388 x 1040 pixel resolution) and ZEN imaging software (from Zeiss) were used to analyze the histology slides. The media thickness, lamellar unit thickness, and number of elastic lamellae were measured using the ZEN software.

MPLSM Images

Stacks of MPLSM images taken through the thickness of the aorta wall were processed into 3D models and analyzed using Amira Resolve RT software (FEI Company).

The media thickness, lamellar unit thickness, number of elastic lamellae, and elastic lamella thickness were measured at three places on each cross-sectioned surface of each scan, for a total of six locations per scan, and an average value calculated. The thickness of the media, lamellar unit, and elastic lamella varies with circumferential and longitudinal stretch ratio when the tissue is deformed under pressure. A correction factor was used to convert the dimensions from the deformed state (which were different for the thoracic and abdominal aortas) to the undeformed state of each aorta. Assuming the aorta wall deforms at a constant volume, such that

$$\lambda_\theta \times \lambda_z \times \lambda_h = 1 \tag{5}$$

where λ_θ is the circumferential, λ_z is the longitudinal, and λ_h is the radial stretch ratio respectively. The radial stretch ratio is

$$\lambda_h = \frac{h}{H} \tag{6}$$

where *h* is the thickness in the deformed state and *H* is the thickness in the undeformed state. Combining Equations 5 and 6, the undeformed thickness was calculated as

$$H = h \times \lambda_\theta \times \lambda_z \quad (7)$$

The volume of the total scan is known (black area in Figure 12 a) and the volume of the elastin in the scan (the green in Figure 12) is easily calculated by Amira. However, the volume of the sample itself (elastin plus spaces within the sample) had to be calculated. The volume above and below the sample in one slice (the yellow in Figure 12) was measured for 11 slices. This value was then used to calculate the volume above and below the sample for all 1024 slices. This volume above and below the sample was subtracted from the scan volume to give the volume of the sample. The surface area of elastin in each scan was calculated by Amira.

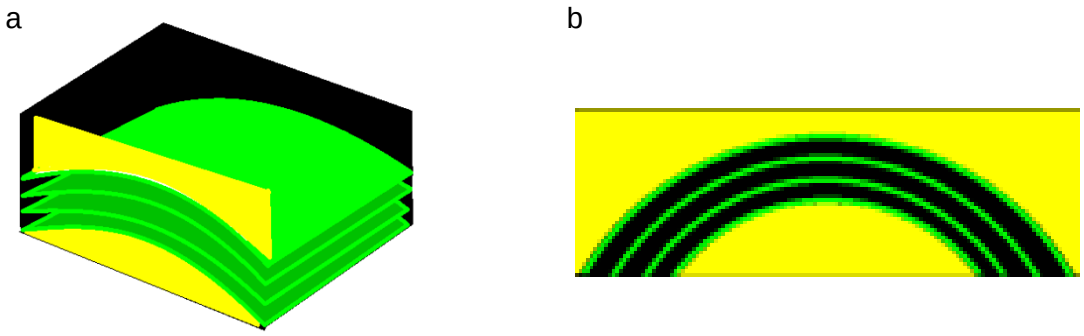

Figure 12. Diagram of elastin in the aorta media. Elastin is green. The yellow areas show the volume above and below the sample in one slice of the 1024 slices that make up the sample. This volume was used to calculate the volume of the sample (elastin and the spaces within the elastin). (a) oblique view (b) cross-sectional view.

Statistical Analysis

Data are reported as means ± 95% confidence intervals. A one-way ANOVA (using VassarStats software) was used for the statistical analysis of the aorta morphology. Statistical significance was assumed at $P<0.05$.

Results

Mechanical Testing

Force-displacement data were collected for intact tissue and purified elastin tissue that had been autoclaved for 4 h. The rationale for selecting 4 h as the standard is presented below (see Autoclaving Time pg. 33). The initial length of the rings decreased by about 10% on autoclaving. Typical loading and unloading curves are shown in Figure 13 for intact thoracic and abdominal samples. The plots also show the data after the 18 cycles have been averaged and smoothed with a 5-point running average (see Figure 13). The curves show an initial increase in force at low displacement (0 – 0.15 mm in the thoracic) that corresponds to the ring being deformed from a circular cross-section but before the ring is stretched (see Figure 14). That is followed by a region of linearly increasing force (0.2 – 0.5 mm in the thoracic) where the elastin is being stretched. In the intact rings, this region is followed by a great increase in force with increasing displacement (0.5 – 0.8 mm in the thoracic) where the collagen is being recruited. In both the thoracic and abdominal aorta rings, the force in the intact ring is larger than that in the purified elastin ring for any given displacement.

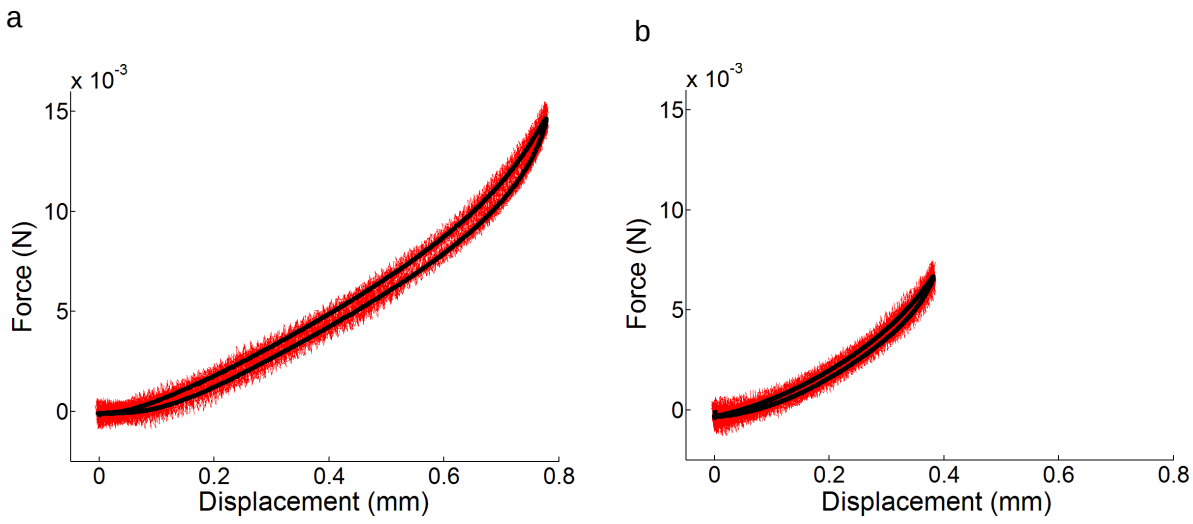

Figure 13. Force-displacement loading and unloading curves for an intact thoracic (*6int*) (a) and abdominal (*ilia*) (b) aorta ring.Red lines show data for cycles two through 19. Black line shows data after averaging the cycles and performing a 5-point running average.

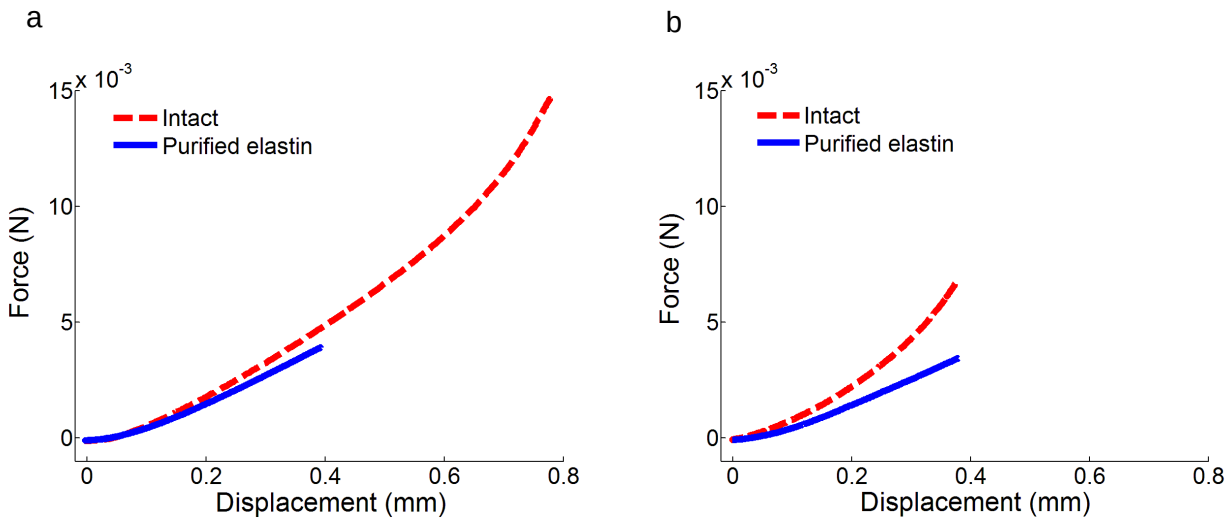

Figure 14. Effect of autoclaving on force displacement loading curves for a thoracic (*6int*) (a) and abdominal (*ilia*) (b) aorta ring before autoclaving (red dashed line) and after 4 h of autoclaving (blue solid line).

To convert force to stress I considered two ways of defining area, and to convert displacement to stretch ratio I considered three ways of defining initial length. Below, I first evaluate stress using the regression method of defining initial length, and second evaluate initial length using the engineering method of defining area.

Engineering stress was calculated by Equation 3 (see Figure 15 a and b) and lamellar stress by Equation 4 (see Figure 15 c and d). Data for the number of elastic lamellae and thickness of the lamellae are presented on page 41. The shape of the stress-stretch ratio loading curves is the same for both normalizing methods but the values of the stress at any stretch ratio are about 80% lower when using Equation 3. As with the force-displacement curves, there are three distinct regions in the stress-stretch ratio curves for intact rings: an initial increase in modulus (at a stretch ratio of 1) corresponding to bending of the ring, a constant modulus (from a stretch ratio of 1.1 to 1.35) corresponding to elastin stretching, and a final increase in modulus (above 1.35 stretch ratio) corresponding to collagen recruitment (see Figure 15). The purified elastin rings only exhibit the first two of those regions as collagen has been removed by the autoclaving. For both thoracic and abdominal aorta rings, at any given

stretch ratio, the stress in the purified elastin ring is lower than that in the intact ring (17% lower in the thoracic and 21% lower in the abdominal aorta at a circumferential stretch ratio of 1.22).

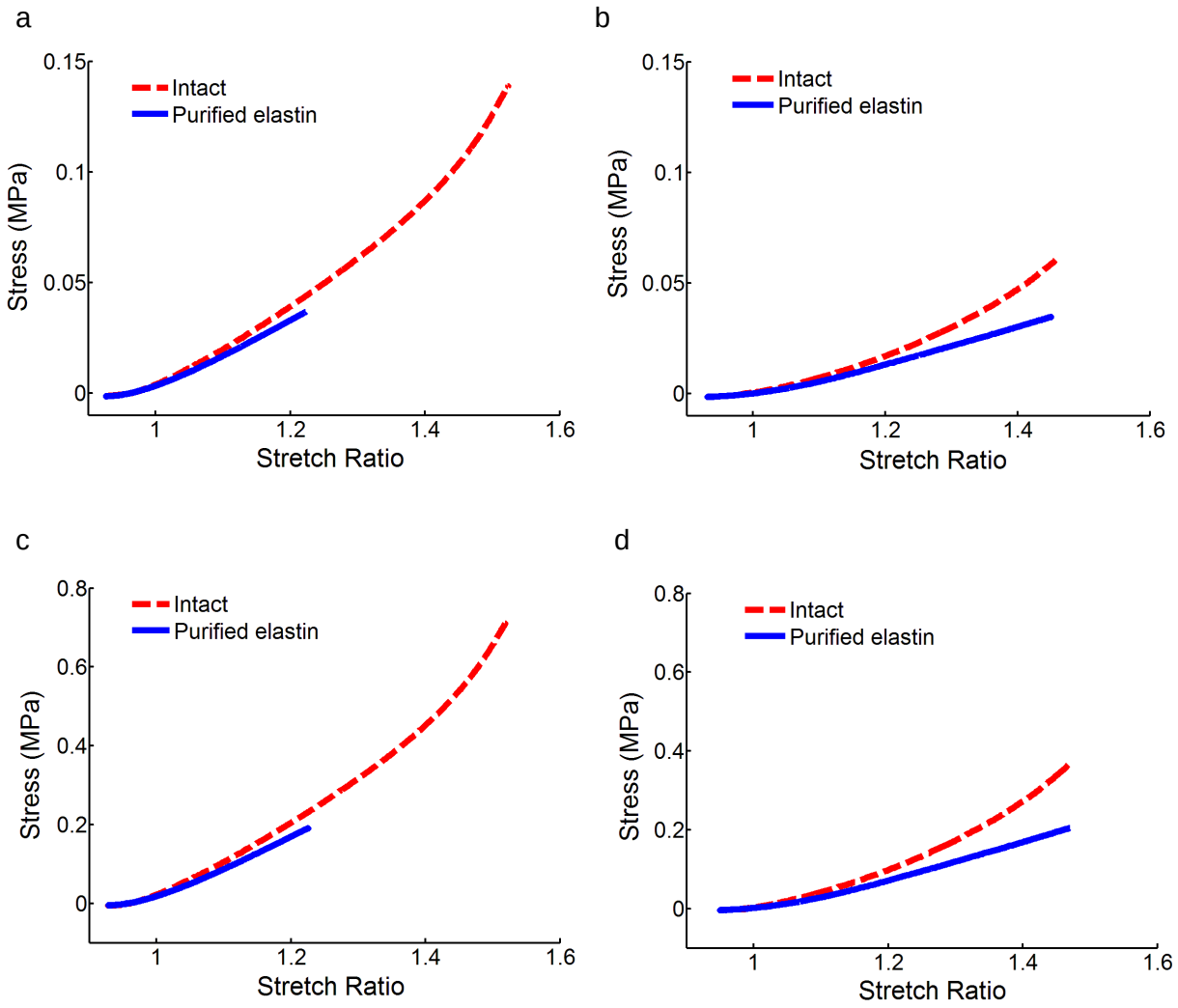

Figure 15. Stress-stretch ratio curves for a thoracic (*6int*) (a,c) and abdominal (*ilia*) (b,d) aorta ring before autoclaving (red dashed line) and after autoclaving (blue solid line). Stress was calculated by normalizing the force by the cross-sectional area as in equation 3 (a,b) and by the width, number of elastic lamellae and thickness of lamellae as in equation 4 (c,d) of the autoclaved ring.

The elastic modulus of the intact and purified elastin aorta rings were calculated from both the engineering stress-stretch ratio curves (Equation 3) and lamellar stress-stretch ratio curves (Equation 4) (see Figure 16 a and b and the Appendix). The latter corrects for the space in the sample and gives a value for modulus closer to that of a single elastin fibre (1.2 MPa; Aaron and Gosline, 1981). The two normalizing methods give the same trends in modulus: both show a constant modulus through all thoracic rings (*1int*, *6int*, *9int*) and the most proximal

abdominal (*acel*) ring, a decrease in modulus in the *lumb* ring, and greater decrease in the *ilia* (most distal) ring. For both normalizing methods and for both intact and purified elastin rings, there was a clear longitudinal trend; the modulus of the most distal ring (*ilia*) was significantly different from that of the thoracic and *acel* rings. When normalized by Equation 3 (cross-sectional area) the *ilia* modulus (0.15 ± 0.04 MPa and 0.12 ± 0.02 MPa) was 42% and 43% lower than the *6int* modulus (0.26 ± 0.03 MPa and 0.21 ± 0.02 MPa) in the intact and purified elastin rings, respectively. When normalized by Equation 4 (elastic lamellae) the *ilia* modulus (0.60 ± 0.07 MPa and 0.47 ± 0.03 MPa) was 32% and 34% lower than the *6int* modulus (0.88 ± 0.09 MPa and 0.71 ± 0.05 MPa) in the intact and purified elastin rings respectively.

The modulus of the intact rings was significantly greater than that of the purified elastin rings at all axial positions. When normalized by Equation 3, the purified elastin ring moduli were on average 22% and 25% lower than the intact ring moduli in the thoracic and abdominal aorta respectively.

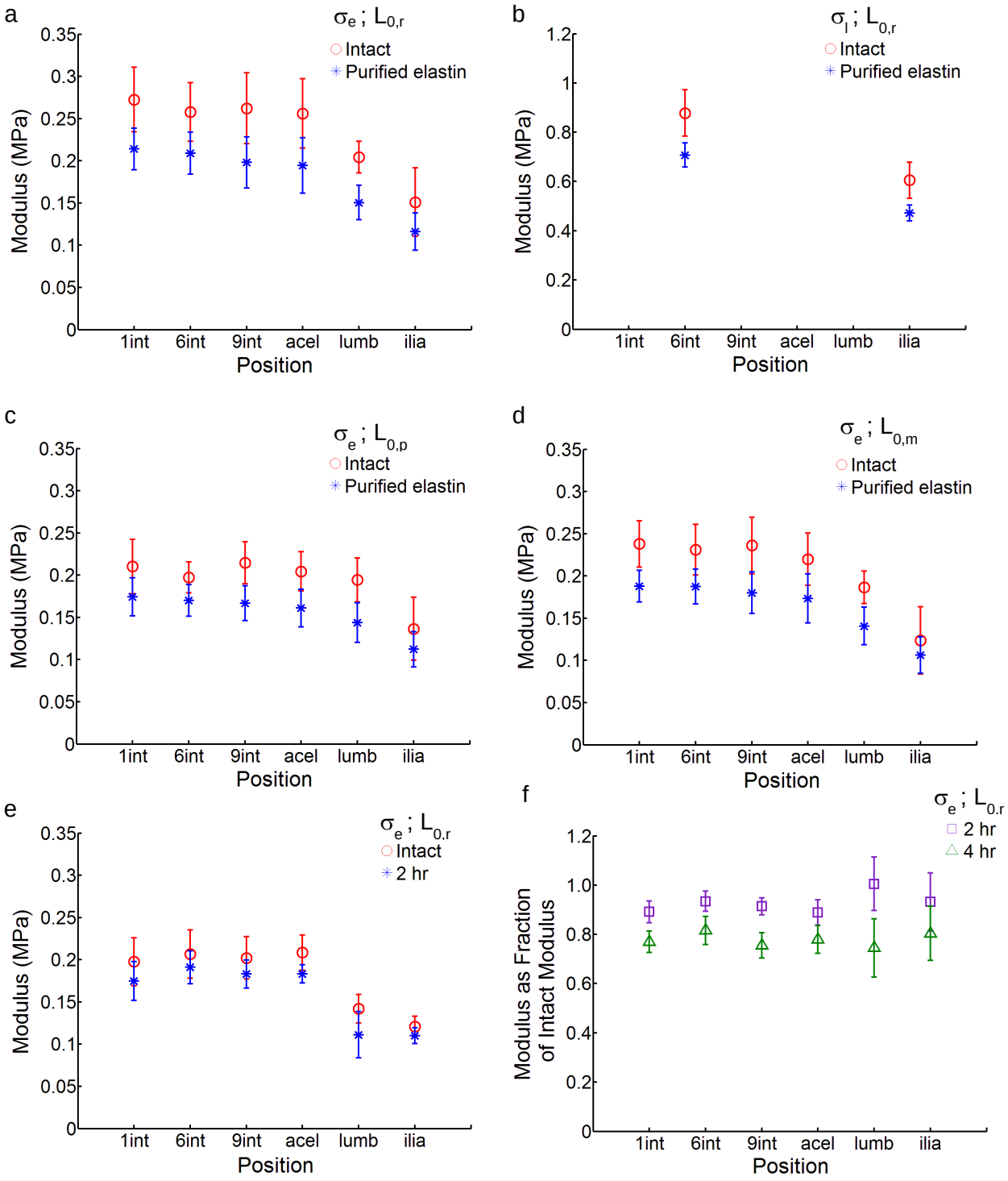

Figure 16. Impact of stress definition, initial length, and autoclave time on elastic modulus of mouse aorta rings at six positions along the aorta, three in the thoracic (*1int*, *6int*, *9int*) and three in the abdominal (*acel*, *lumb*, *ilia*). Red circles are intact rings (before autoclaving) and blue stars are purified elastin rings (after autoclaving for 4 hr unless otherwise specified). (a) Stress was from engineering stress; stretch ratio was from regression initial length. (b) Lamellar stress; regression initial length. (c) Engineering stress; morphological initial length. (d) Engineering stress; mechanical initial length. (e) Engineering stress; regression initial length. Autoclave time was 2 hr. (f) Engineering stress; regression initial length. Modulus of rings autoclaved for 2 and 4 hours as a fraction of their intact modulus. Means ± 95% CI. n = 9 for all intact rings. For purified elastin rings, n = 9 (*9int* and *lumb*), n = 8 (*6int*, *acel* and *ilia*), and n = 7 (*1int*). (a-e) Purified elastin *ilia* significantly different from *1int*, *6int, 9int*, and *acel*.

Initial Length

The initial lengths of one representative purified elastin thoracic ring were 1.14 mm, 1.16 mm, and 1.34 mm and for one purified elastin abdominal ring were 0.76 mm, 0.66 mm, and 0.76 mm as calculated by the morphological, mechanical, and regression method respectively (see Table 3).

Aorta	Initial Length Calculation Method		
	Morphological (mm)	Mechanical (mm)	Regression (mm)
Thoracic (*6int*)	1.14	1.16	1.34
Abdominal (*ilia*)	0.76	0.66	0.76

Table 3. Initial lengths of mouse aorta purified elastin rings as calculated by three different methods: morphological, mechanical, and regression. Values are from one thoracic and one abdominal ring to compare the three methods.

Figure 16 a, c, and d show the impact of initial length definition on modulus using engineering stress. When the initial length determined by the morphological method was used to calculate the stretch ratio (see Figure 16 c), the moduli of the abdominal *ilia* ring is lower than that of the thoracic and *acel* rings. This trend in modulus is very similar to that when the initial length was determined by the regression method (see Figure 16 a). The modulus of the *ilia* (most distal) intact ring was significantly lower than the modulus of the *1int*, *9int*, and *acel* rings. The modulus of the *ilia* purified elastin ring was significantly lower than the modulus of the four most proximal rings (*1int*, *6int*, *9int*, and *acel*). The *ilia* modulus (0.14 ± 0.04 MPa and 0.11 ± 0.02 MPa) was 30% and 35% lower than the *6int* modulus (0.20 ± 0.02 MPa and 0.17 ± 0.02 MPa) in the intact and purified elastin rings, respectively.

When the initial length determined by the mechanical method was used to calculate the stretch ratio (see Figure 16 d), the elastic modulus was significantly lower in the *ilia* (most distal) ring compared with the four most proximal rings (*1int, 6int, 9int,* and *acel*) for both the intact and purified elastin. The *ilia* modulus (0.12 ± 0.04 MPa and 0.11 ± 0.02 MPa) was 48% and 42%

lower than the *6int* modulus (0.23 ± 0.03 MPa and 0.19 ± 0.02 MPa) in the intact and purified elastin rings, respectively.

The regression initial length has been selected as the standard as it was deemed to be the least subjective (see Initial Length discussion pg. 46).

Autoclave Time

The stiffness of each ring decreased progressively with autoclaving time. For each ring, the spring constant at each autoclave time was normalized by the spring constant at autoclave time 0 hr (intact). Figure 17 shows that the spring constant decreased linearly with increasing autoclave time. The spring constant decreased by 14, 18, 30, and 52% after autoclave times of 1, 2, 4, and 8 hours, respectively, compared with the intact value. The initial decrease is presumably due to removal of collagen and smooth muscle, but with longer autoclaving times elastin degradation can occur (Lillie et al., 1994).

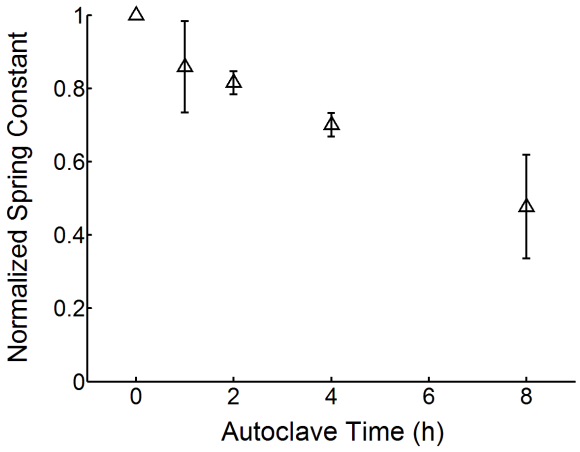

Figure 17. Effect of autoclave time on spring constants of mouse aorta rings. Spring constants are normalized by the value at time 0 hr (intact). Means ± 95% CI, n = 54, 6, 36, 51, and 11 for 0, 1, 2, 4, and 8 hours respectively.

The elastic modulus of the rings show the same longitudinal trend when autoclaved for two hours (see Figure 16 e) as when autoclaved for four hours (see Figure 16 a). The moduli of the two most distal rings, *lumb* (1.03 ± 0.08 and 0.79 ± 0.07 MPa, intact and two-hour autoclaved, respectively) and *ilia* (0.95 ± 0.11 and 0.69 ± 0.06 MPa, intact and two-hour

autoclaved, respectively), were significantly lower than that of the thoracic and *acel* rings (means 1.33 ± 0.11 and 1.09 ± 0.10, intact and two-hour autoclaved, respectively). The *ilia* modulus was 30% and 40% lower than the *6int* modulus in the intact and two-hour autoclaved rings, respectively. Note that a different set of rings was autoclaved for two hours so the data for intact rings is from different rings in Figure 16 a and e, although the longitudinal trend is the same in both sets of data.

The moduli of the purified elastin rings after autoclaving for two and four hours have been expressed as a percent of the moduli of the intact rings (see Figure 16 f). The moduli dropped on average 8% and 22% after two and four hours of autoclaving respectively.

Four hours has been selected as the standard autoclaving time for the mouse aorta rings as it was deemed to be the time at which the collagen had been denatured and washed away but the elastin had not been significantly affected (see Autoclave Time discussion pg. 49).

Effect of Mouse Age and Weight

Neither age nor weight had an effect on the elastic modulus of the rings (see Figure 18). The youngest mouse in this study was 34 d old, by which time the mechanical properties of mouse arteries are stable (Huang et al., 2006).

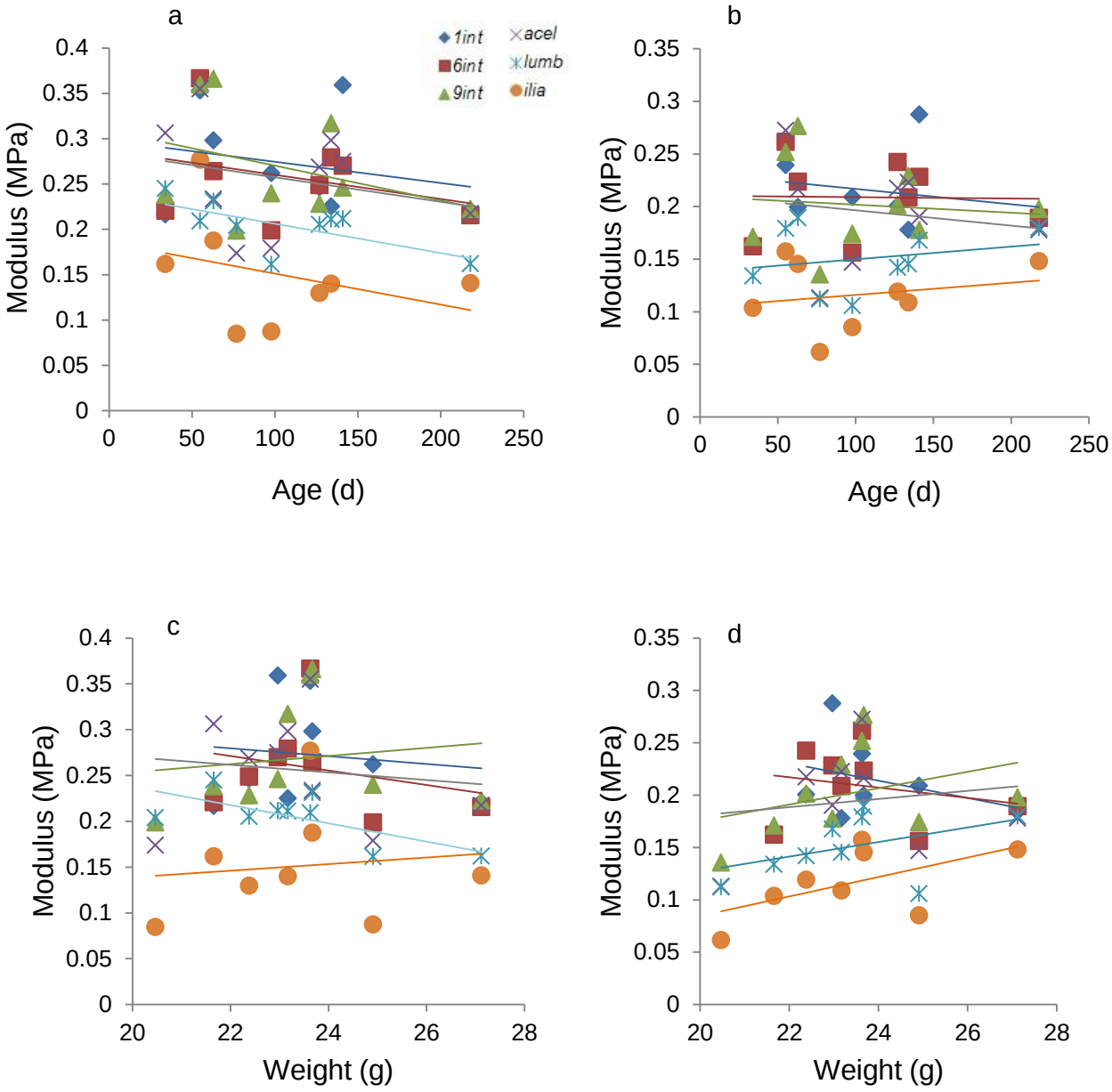

Figure 18. Effect of age and weight on elastic modulus of mouse aorta rings.Age (a,b) and weight (c,d) elastic moduli are shown for intact (a,c) and purified elastin (b,d) aorta rings. Data points are individual samples. Lines are linear regressions.

Morphology

Histology

Cross-sections of the thoracic and abdominal aortas show collagen in the adventitia and elastic lamellae in the media with collagen and smooth muscle cells interspersed (see Figure 19). The mostly straight elastic lamellae show that the aorta was fixed close to physiological pressure (MPLSM data of aortas at low inflation pressure showed wavy elastic lamellae). The

media was 22.6 µm thick in the thoracic and only 13.0 µm thick in the abdominal aorta (see Table 4). The lamellar unit thickness in this aorta was slightly larger in the thoracic (5.1 µm) than in the abdominal aorta (4.0 µm). At least part of the difference in medial thickness and lamellar unit thickness may be due to differences in stretch ratios on inflation. Since stretch ratio was not measured for this aorta the thoracic and abdominal values cannot be compared. There were 5.3 elastic lamellae in the thoracic and 4.0 in the abdominal aorta. The fraction of a lamella results from the elastic lamella splitting into two in some areas and merging back into one in others, resulting in some areas of the circumference having five lamellae and some having six.

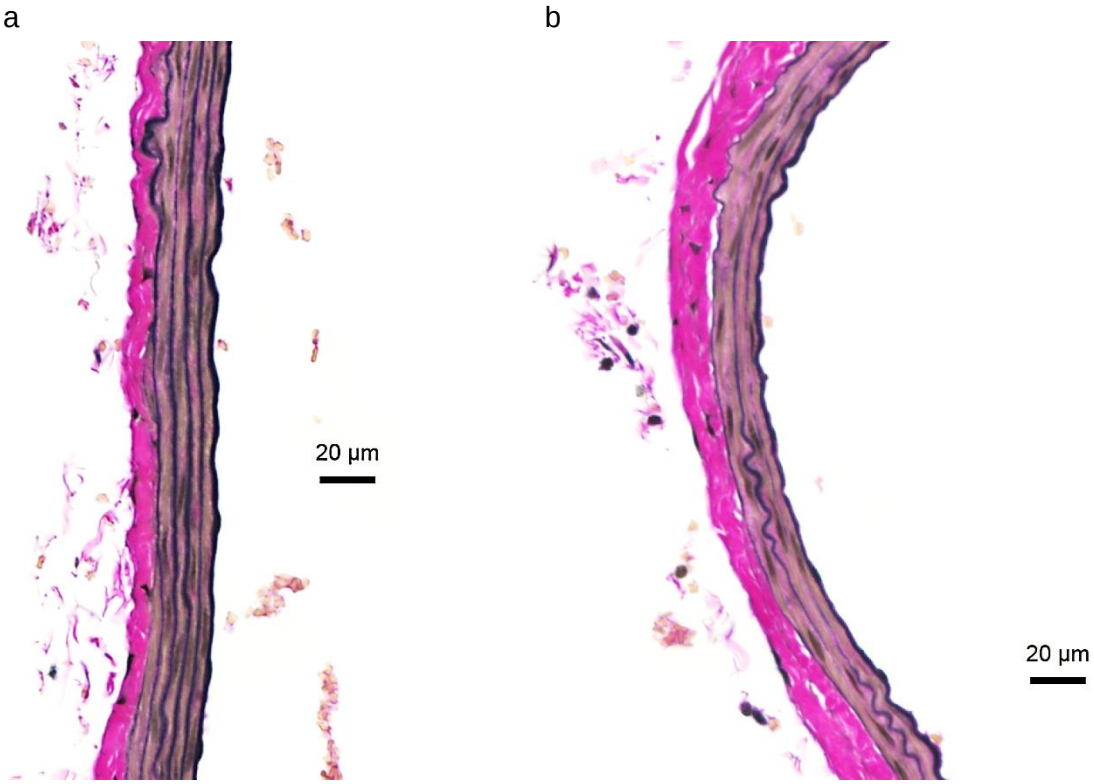

Figure 19. Light microscopy cross-section of the aorta wall after infusing with glutaraldehyde fixative under pressure. (a) thoracic aorta, (b) abdominal aorta; elastin is black, collagen is magenta, and smooth muscle cells are brown. Van Gieson's stain.

Aorta	Media Thickness (μm)	Number of Elastic Lamellae	Lamellar Unit Thickness (μm)
Thoracic	22.6	5.3	5.1
Abdominal	13.0	4.0	4.0

Table 4. Aortic media measurements from histology sections of intact aortas at approximately physiological pressures. Thoracic: n = 2, abdominal: n = 1.

Stretch Ratio

The circumferential stretch ratios of one aorta tested at the mouse's mean physiological pressure were 1.37 and 1.55 in the thoracic and abdominal aortas respectively. The mean circumferential stretch ratios of the aortas after agarose injection were 1.32 ± 0.10 and 1.21 ± 0.14 for the thoracic and abdominal aortas respectively (see Table 5). The mean longitudinal stretch ratios of the aortas after agarose injection were 1.11 ± 0.04 and 1.08 ± 0.03 for the thoracic and abdominal aortas respectively (see Table 5). These differences will have an impact on morphology and must be taken into account (see Stretch Ratios and Inflation Pressure discussion pg. 47).

Inflation	Circumferential Stretch Ratio		Longitudinal Stretch Ratio	
	Thoracic	Abdominal	Thoracic	Abdominal
PBS Inflation to 105 mm Hg	1.37	1.55	NA	NA
Agarose Inflation	1.32 ± 0.10	1.21 ± 0.14	1.11 ± 0.04	1.08 ± 0.03

Table 5. Circumferential and longitudinal stretch ratios of mouse aortas as calculated by inflation with PBS solution to mean physiological pressure and after inflation with agarose. Means ± 95% CI, PBS inflation: n = 1; circumferential thoracic: n = 8, abdominal: n = 7, longitudinal thoracic: n = 4, abdominal: n = 6.

Multiphoton Laser Scanning Microscopy

Images from MPLSM of the thoracic aorta show adventitial collagen and medial elastin (see Figure 20 d and f). Adventitial collagen had been removed from the abdominal aorta before imaging so only elastin is visible in those scans (see Figure 20 e and g). Contrary to what was expected, there is no collagen visible in the media, presumably because it was not detected by

the MPLSM. This thesis focused on the mechanical properties of elastin so not being able to visualize the medial collagen in the MPLSM images was not a hindrance.

Individual image slices (see Figure 20 a and b) are used to reconstruct a 3D model of the aorta wall (see Figure 20 d - g). Elastic lamellae can be seen, as well as some interlamellar elastin including elastin struts (see Figure 21).

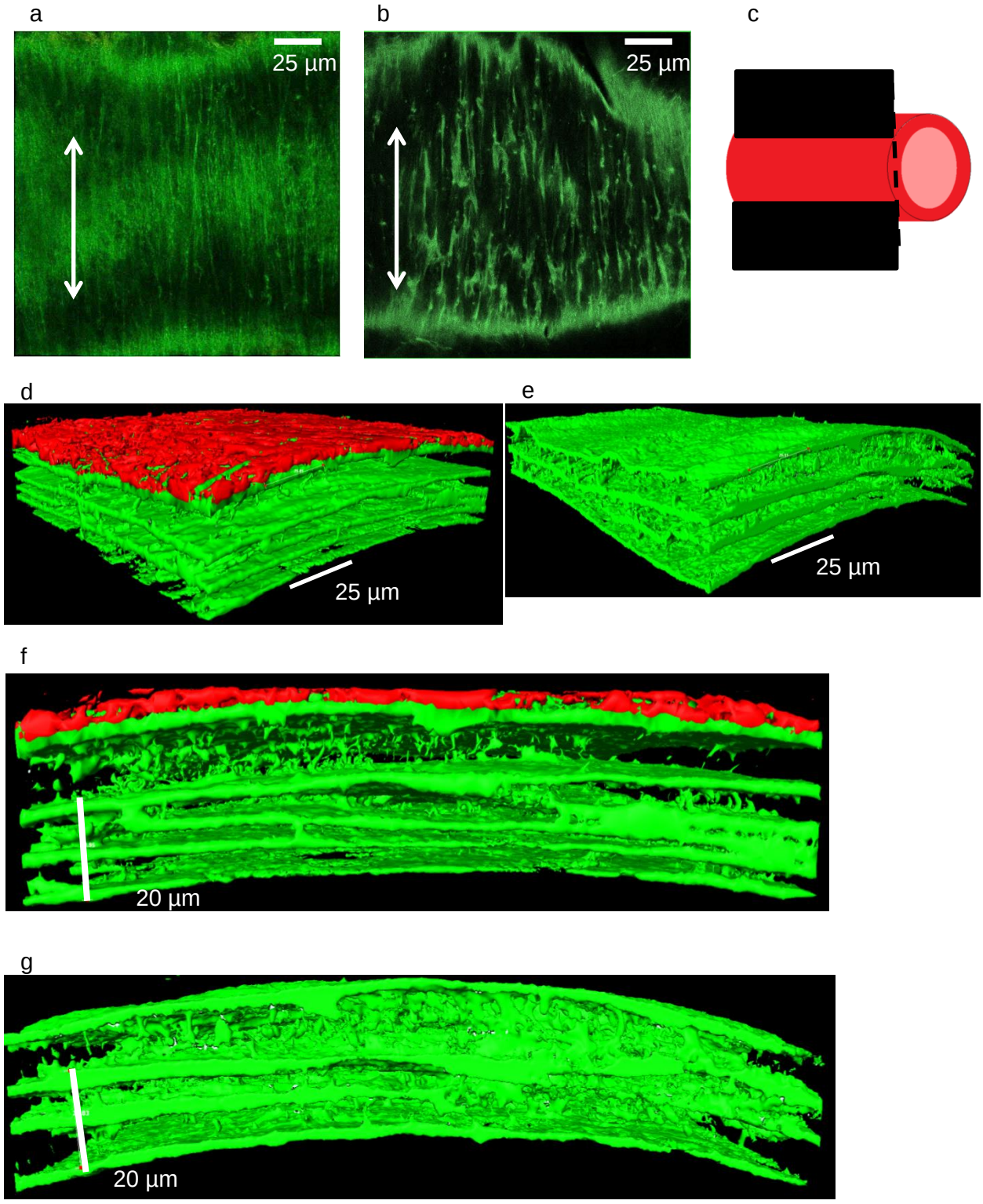

Figure 20. MPLSM images of the mouse aorta wall showing collagen (red) and elastin (green). Image of one slice of the stack of images of the thoracic (a) and abdominal (b) aorta taken in the orientation as shown in (c). White arrows indicate the circumferential direction. 3D reconstructions of the stack of images from an oblique view from above (d, e) and cross-section (f, g) of the thoracic (d,f) and abdominal (e,g) aortas.

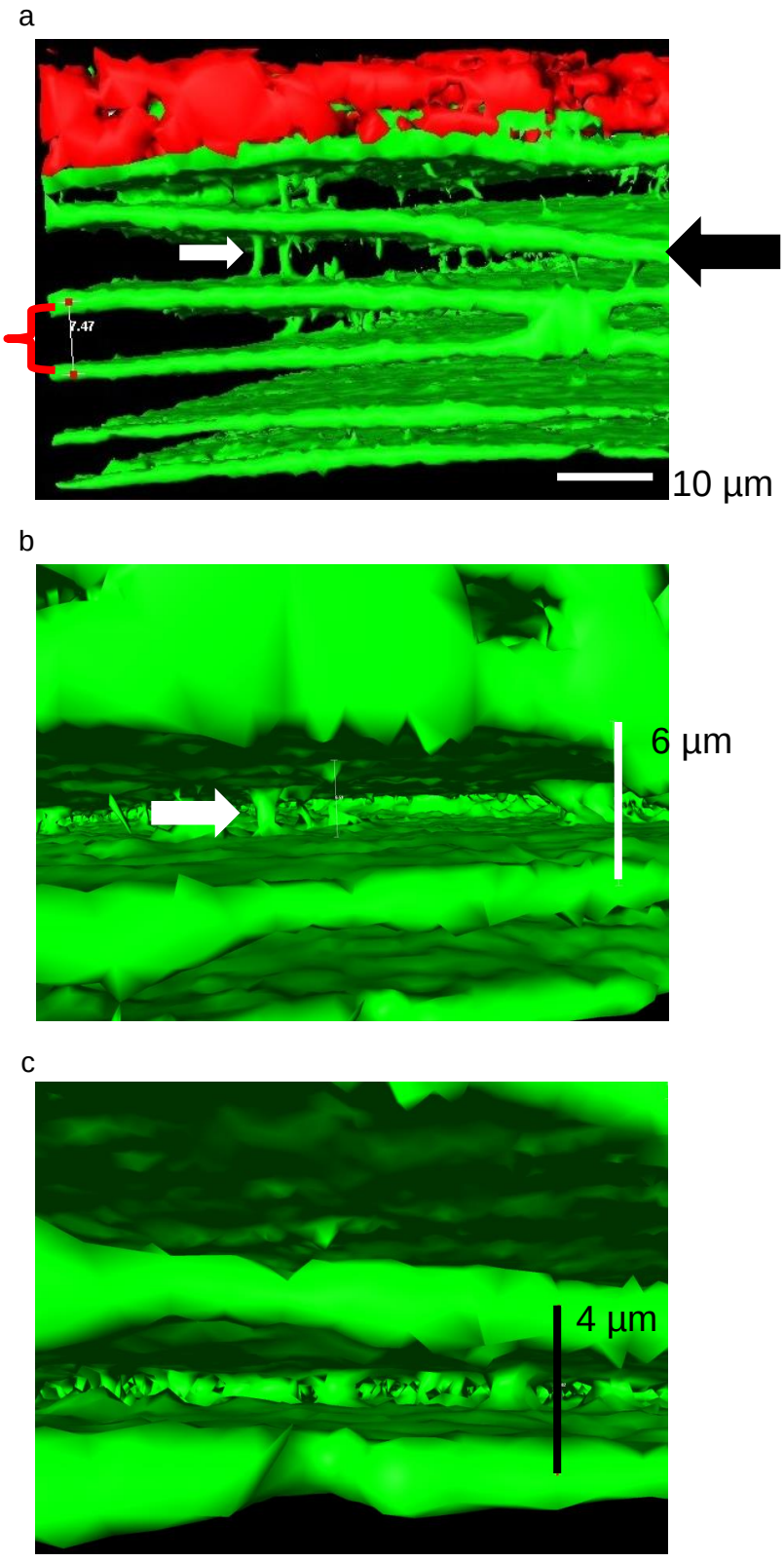

Figure 21. MPLSM images of elastin structures in the mouse aorta wall. Elastin is green; collagen is red. (a) Close-up view of one section of thoracic aorta indicating one lamellar unit (red bracket), a strut (white arrow), and an elastic lamellae (black arrow). (b) White arrow shows a strut. In some areas the struts are easily counted (b) but in some they are not (c).

The mean media thicknesses of the undeformed thoracic (40.2 ± 6.8 μm) and abdominal (37.6 ± 7.5 μm) aortas were not significantly different (see Figure 22 a) although there was much variation between individual animals (see Figure 22 b). The values obtained in this study for the deformed (pressurized) thoracic media thickness (22.6 μm and 27.6 μm from histology and microscopy respectively; see Table 4 and Table A-11 in the Appendix) are in agreement with that found by Wolinsky and Glagov (30 μm; Wolinsky and Glagov, 1967).

The undeformed lamellar unit thickness was significantly smaller (by 30%) in the thoracic aorta than in the abdominal (8.8 ± 1.3 μm and 12.7 ± 2.7 μm respectively) (see Figure 23 a). The mean lamellar unit thicknesses of the thoracic aorta were 5.1 μm and 6.1 μm from histology (see Table 4) and MPLS microscopy (in the deformed state, before the correction for stretch; see Table A-11 in the Appendix), respectively, which are in agreement with Wolinsky and Glagov's value of 6 μm (Wolinsky and Glagov, 1967). The volume fraction of elastin was significantly higher (by 67%) in the thoracic aorta than in the abdominal (0.5 ± 0.1 μm and 0.3 ± 0.1 μm respectively) (see Figure 23 b). The elastic lamella thickness was not significantly different between the thoracic (2.7 ± 0.2 μm) and abdominal (2.8 ± 0.4 μm) aorta (see Figure 23 c). There were 5.6 elastic lamellae in the thoracic aorta and 4.0 in the abdominal (see Figure 23 d). There was no significant difference between the thoracic and abdominal aortas in either the surface area of elastin normalized by the number of elastic lamellae (0.067 ± 0.010 mm^2 and 0.074 ± 0.011 mm^2 respectively) or the surface area of elastin normalized by the elastin volume (1.0 ± 0.2 μm^{-1} and 1.4 ± 0.4 μm^{-1} respectively) (see Figure 23 e and f).

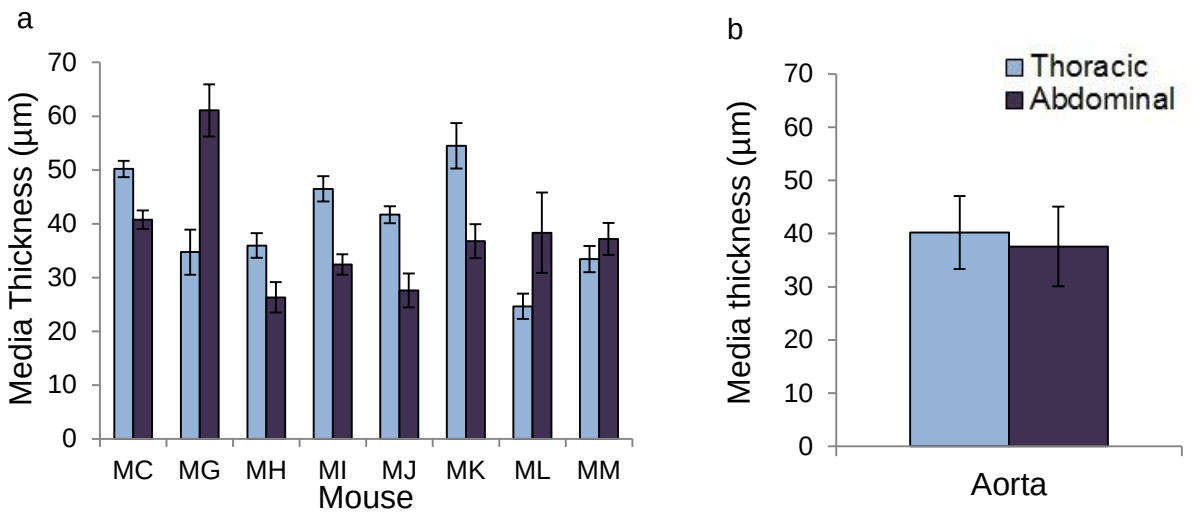

Figure 22. Media thickness of the unloaded aorta wall as determined by MPLSM images for mice MC – MM. Means of measurements at six points within one location per mouse (a) and means of all mice (b) ± 95% CI. Values represent the aorta wall in the unloaded state.

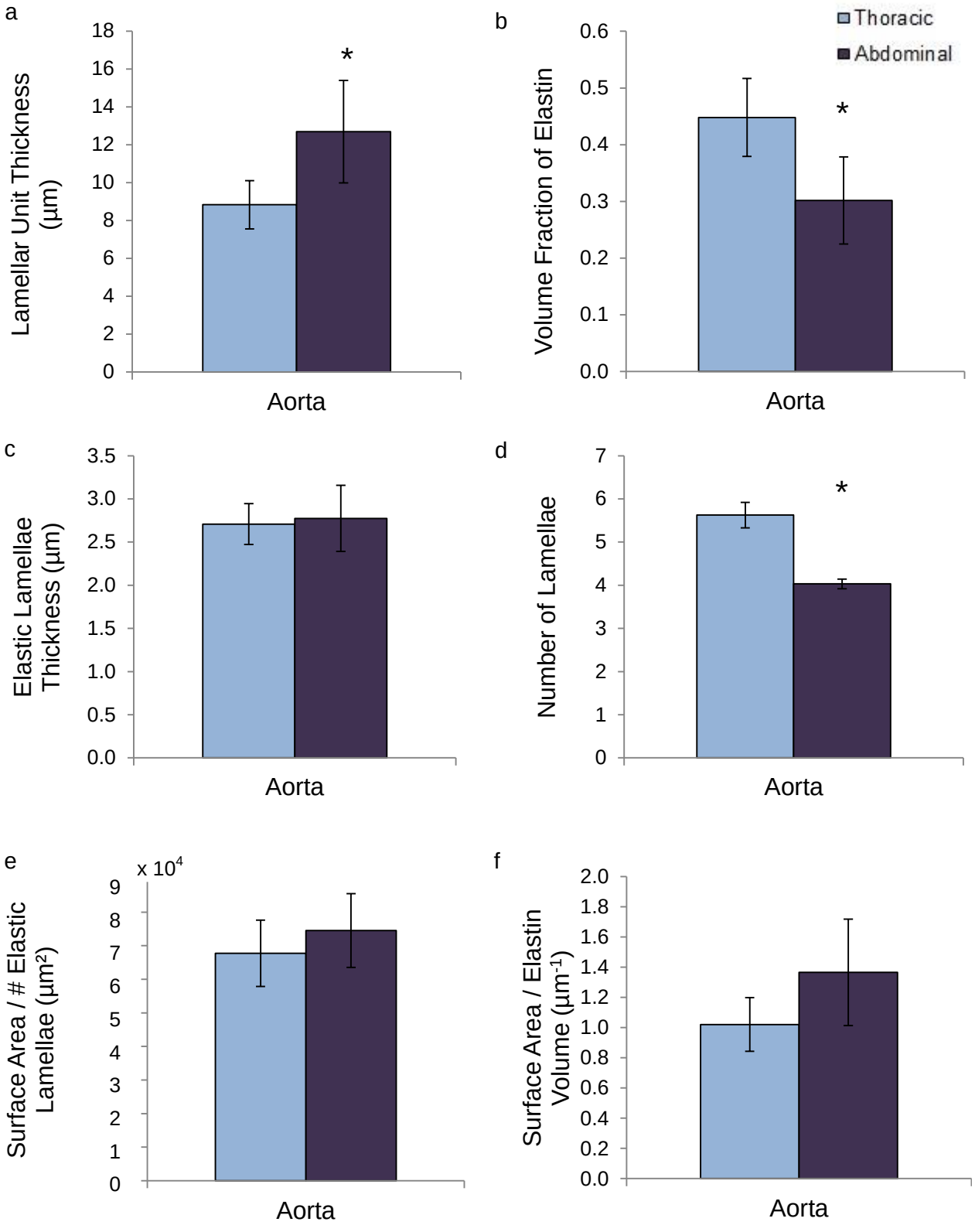

Figure 23. Measurements of the mouse aorta media as determined by MPLSM images. Lamellar unit thickness (a), volume fraction of elastin (b), elastic lamellae thickness (c), number of elastic lamellae (d), surface area normalized by the number of elastic lamellae (e) and surface area normalized by the elastin volume (f) for thoracic and abdominal mouse aortas. Means ± 95% CI, n = 8. Values in (a) and (c) represent the aorta wall in the unloaded state. * represents statistical significance.

Discussion

The validity of the data and methods used to normalize the data are first discussed, followed by a discussion of the four hypotheses.

Analyzing the Data

This study required relatively large thoracic aortas to be compared to much smaller (by 30-50%) abdominal aortas and intact elastin rings to be compared to purified elastin rings. It is critical to establish that differences in the reported moduli represent material properties of the aortas and not differences due to size. The size difference is dealt with in part by normalizing the data according to the dimensions of the rings but size also led to some difficulties in the techniques that were used. Comparing intact and purified elastin rings has its own difficulties and also implies knowledge of the autoclave time used to produce a purified elastin ring.

Comparisons of Size – Large and Small

Techniques

Mechanical testing was difficult because the rings are small. One set of hooks could not be used for all aorta rings because the larger hooks were too large to fit in the abdominal aorta rings and the small hooks cut into the thoracic aorta rings because of their relatively small diameter. The relative error in the measurements is also different for each aorta because of their different sizes.

Normalizing Force and Displacement

The aorta rings were not all the same size and so in order to compare the mechanical properties of a smaller ring to a larger ring the force and displacement data had to be normalized for the dimensions of each ring. This was the main challenge in the mechanical testing part of this thesis and care had to be taken to ensure artefacts weren't introduced when normalizing the data. There is more than one way to calculate the cross-sectional area used to normalize the force and more than one way to calculate the initial length used to normalize the

displacement, and different values are obtained (for the same elastin) depending on the method used. Each method has its own assumptions; these assumptions and the chosen method are discussed below.

Cross-sectional Area

The conventional method of calculating stress is to normalize force by the cross-sectional area of the material being stretched (see Equation 3). This thesis uses the engineering stress (non-deformed cross-sectional area) not the true stress (deformed cross-sectional area) to avoid the possibility of introducing artefacts through a second use of the initial length of the ring (which is used to calculate the stretch ratio). When this conventional normalizing method is used for an aorta wall, the spaces between the elastic lamellae are also included in the cross-sectional area, resulting in a stress, and therefore also a modulus, that is much smaller than what it would be if the cross-sectional area of only the elastin was used. One way to resolve this is to correct for the fibre packing density of elastin; however, this was not done because the error in measuring density in such small samples was prohibitively high and could possibly have introduced a size-based bias. Instead, the force was normalized by the area of elastin as determined by MPLSM data. Wall thickness was based on the number of elastic lamellae and average lamellar thickness (see Equation 4). Excluding the spaces between the elastic lamellae brought the resultant moduli close to that of a single elastin fibre (1.2 MPa; Aaron and Gosline, 1981) (see Figure 16 b).

Regardless of the stress calculation used, modulus decreased with distance from the heart. The modulus of the most distal ring (*ilia*) was significantly lower than that of the four most proximal (thoracic and *acel*) rings and the modulus of the second most distal ring (*lumb*) was between that of the proximal and *ilia* rings (see Figure 16 a and b). As was observed in the pig thoracic aorta, there is a clear regional difference in elastin mechanics (Lillie and Gosline, 2007).

Initial Length

Knowing the initial length of each ring is critical for calculating the stretch ratio of the ring and therefore also the ring's modulus. To ensure an appropriate value was obtained, the initial length was calculated using three different methods: morphological, mechanical and regression length. Each method resulted in a slightly different value of initial length (see Table 3).

The morphological initial length relied on the same amount of PBS solution being wicked out from under the cover slip before the photos of the ring were taken. A different volume of PBS solution under the cover slip would affect how flattened the ring was, and therefore could affect its length. Even with an established protocol this method was subjective.

The mechanical initial length relied on the experimenter determining by observation (with the help of a magnifying glass) at what displacement of the tensile tester the sides of the ring just became parallel. Due to the difficulty of accurately determining this point on such a small object, this method was thought to be the least accurate; however, a method was required that could be done during the experiment without handling the tissue as required for morphological length. It provided an initial length from which the maximum stretch (1.5) was calculated during the tensile testing.

The initial length by regression represents the length at which the bulk of elastin started to resist deformation (Lillie et al., 1994). This method relied almost entirely on data from the tensile tester; the experimenter only determined the region of the force-length curve where it has a constant slope, a task that was very reproducible on the force-length curve of a purified elastin ring. This method of calculating the initial length was therefore used throughout the data analysis because it was deemed to be the least subjective.

Regardless of the initial length used, the modulus of the most distal purified elastin ring (*ilia*) was consistently significantly lower than that of the thoracic rings (see Figure 16 a, c, and d). The purpose of this study was not to determine the definitive elastic modulus of aortic rings,

but to look for differences in the modulus at various positions along the aorta. There is a clear trend with all initial lengths of decreasing modulus with distance from the heart, showing that the trend is not due to artefacts introduced when calculating the stretch ratio.

Stretch Ratios and Inflation Pressure

I investigated the morphology of the elastin in the aorta wall to identify whether any difference in the thoracic and abdominal aortas could account for the 43% difference in elastic modulus of purified elastin rings measured in uniaxial tensile tests (which are independent of pressure). Preliminary MPLSM tests of unpressurized aortas gave poor results, in part because of the increased thickness of the wall in the unloaded state, so subsequent MPLSM was done with the aortas in a loaded state. The physiological stretches (both circumferential and longitudinal) are different in the thoracic and abdominal aorta, and any difference in stretch had to be taken into account in the morphology measurements. Although I aimed to obtain physiological pressures to help in understanding mouse physiology, the exact pressure used for this part of the study is immaterial since the dimensions were corrected to the unloaded state.

Aldehydes (formaldehyde or glutaraldehyde) are commonly used as a tissue fixative but they are not compatible with MPLSM because they fluoresce and mask the autofluorescence from elastin. As an alternative, agarose gel was injected into the aorta such that the bulk of the gel would physically hold the aorta in a stretched state. However, because the aorta is so small it was difficult to get both the thoracic and abdominal aortas to physiological pressure before the gel set, and it was difficult to monitor the pressure with a pressure transducer. To determine whether the agarose-injected aortas had stretch ratios similar to those under physiological pressure, the stretch ratios of the aortas after agarose injection were compared with the stretch ratio obtained by PBS solution inflation to physiological pressure (see Table 5). The mean circumferential stretch ratio of the thoracic aortas was within 4% of that at physiological pressure but was 31% lower than previously reported values in mouse tissue (1.96 and 1.9; Guo and Kassab, 2003; Huang et al., 2006). The mean circumferential stretch ratio of the

abdominal aortas was 22% lower than that at physiological pressure and approximately 33% lower than previously reported values (1.74 and 1.8; Guo and Kassab, 2003; Huang et al., 2006). The mean longitudinal stretch ratios were 15% and 33% lower than previously reported values for the thoracic and abdominal aortas, respectively, in mouse tissue (1.3 and 1.6; Guo et al., 2002). The lower stretch ratios of the abdominal aortas will have implications on the morphological measurements obtained in this state. The most obvious of these is that the abdominal media, lamellar unit, and elastic lamellae thicknesses will appear spuriously high since the aorta wall becomes thinner at higher pressures (Wolinsky and Glagov, 1964). The problem of the thoracic and abdominal aortas being at different stretch ratios during the MPLSM is dealt with by converting the values in the deformed state to the values in the undeformed state. Assuming the aorta wall deforms at constant volume (Lillie et al., 2010), a correction factor can be calculated to account for the radial stretch when the tissue is stretched in the longitudinal and circumferential orientations. This value can then be used to convert each of the measured thickness values to the value in the undeformed state, allowing the thoracic and abdominal aortas to be compared (see Equations 5-7).

Comparisons of State – Intact and Purified Elastin

Intact arteries have a collagenous adventitial layer whereas it has been removed from purified elastin arteries during autoclaving. This study is concerned with the media but it cannot be directly measured in intact rings because of the surrounding adventitia. For this reason many of the comparisons of intact and purified elastin required for the data analysis are not straightforward.

The initial length of the purified elastin ring was used to calculate the stretch ratio for both the intact and the purified elastin ring. Since the same ring was tested before and after autoclaving and the amount of elastin in that ring does not change, the same initial length was used for both rings. The initial length of the purified elastin ring was used instead of that of the intact ring because the purified elastin ring (which is lacking collagen and smooth muscle cells)

gives a better approximation of the length of the *elastin* in the ring (as opposed to the length of the ring). After autoclaving, the initial length of the rings decreased by about 10% (in both the thoracic and abdominal aortas), presumably because the bulk of the smooth muscle cells holds the elastin out, thereby increasing the length of the ring. When the smooth muscle cells are not there, the elastin recoils and the initial length is decreased. This effect has been seen in other arteries (Lillie et al., 1994) and does not affect the resultant moduli. Since the elastin is stretched by 9% in the intact tissue, the modulus is measured at a 9% higher stretch in the intact than in the purified elastin rings; however, since the curves are linear over a long range, the slope (modulus) is the same.

Autoclave Time

Elastin is covalently cross-linked and is much more robust than collagen so autoclaving aortic tissue denatures and washes away collagen (and smooth muscle cells) long before the elastin is affected (Partridge et al., 1955; Lillie et al., 1994; Gundiah et al., 2007). One of the goals of this thesis is to determine the mechanical properties of elastin along the aorta by testing a purified elastin aorta. It is therefore important to know the autoclave time needed to denature the collagen without affecting the integrity of the elastin to ensure the moduli being compared are those of purified elastin. The moduli of the intact aortas provide a point of comparison to ensure the autoclaving time is appropriate.

There is no published protocol for autoclaving mouse aortic tissue. A previous study of pig aorta rings (Lillie et al., 1994) has shown that collagen denatures into gelatin in about 30 minutes, using tissue shrinkage as the index (Boedtker and Doty, 1956). The gelatin is removed from the tissue by diffusion during further autoclaving. Lillie et al. (1994) used an autoclave time of eight hours, and it is reasonable to assume that a shorter autoclave time would be required for mouse tissue since pig aorta rings are much larger than mouse aorta rings (approximately 20 mm *vs.* 1 mm diameters respectively) and the denatured collagen will diffuse out of a smaller ring more quickly.

Autoclave times of one, two, four, and eight hours were initially used and the resultant ring mechanical properties analyzed to determine the optimal autoclave time. Note that all of these autoclave times are longer than the time required for collagen to be denatured. There was qualitative evidence for collagen no longer being present in the purified elastin rings in that they broke much more easily than the intact rings during tensile testing.

The tensile testing data also provides quantitative evidence for collagen having been removed from the rings. When comparing the loading curves for intact and purified elastin rings (see Figure 14 and Figure 15), the intact curves have an increasing slope (and therefore much increased spring constant and modulus) at higher strains, indicating that collagen has been recruited, whereas the purified elastin curves have a constant slope, even at higher strains, showing no evidence of collagen recruitment. The modulus is taken at low strains before the point where collagen would have been recruited so it shouldn't affect the modulus even if it were still present in the tissue.

There is not a large difference in the normalized spring constants after two and four hours of autoclaving (82% and 70% of the intact spring constant respectively). However, after eight hours the spring constant is much lower (48% of that of the intact) indicating that elastin is being damaged. The fact that many more of the eight-hour autoclaved rings broke during tensile testing than the four-hour autoclaved rings may be evidence of elastin degradation.

Focussing on autoclave times of two and four hours, both times resulted in moduli that were very similar (0.19 vs. 0.21 MPa for *6int* and 0.11 vs. 0.12 MPa for *ilia*, at two and four hours respectively). This is evidence that after two or four hours of autoclaving, collagen has been denatured but the effects on elastin are not enough to significantly alter the moduli. An autoclave time of four hours has been used as the optimum in this study. Since there is more collagen in the distal aorta, the longer time was chosen to be absolutely sure all collagen had been removed.

Comparisons of Ring Positions – Elastic Modulus

The main goal of this study was to investigate the material properties of elastin in the aorta. Elastin is a three-dimensional structure so knowing its mechanical behaviour in three dimensions is important and relates to its *in vivo* physiological conditions. Uniaxial ring tests and cylindrical inflation tests have been shown to produce the same results (Cox, 1983; Lillie et al., 2012); this study used uniaxial ring tests because they were relatively easier to conduct on the small mouse aortas.

Regardless of how the data were normalized and whether the rings were autoclaved for two or four hours, the modulus of purified elastin in the most distal abdominal ring is lower than that in the thoracic (see Figure 16). When using the engineering stress and regression initial length as previously discussed, there is a significant decrease in elastic modulus when comparing the *6int* and *ilia* positions (42% and 43% in intact and purified elastin respectively). This is a large decrease in elastic modulus for a protein that has previously been thought to have constant material properties throughout the aorta.

Previous work in this area by Lillie and Gosline (2007) showed that the elastic modulus of pig thoracic aorta increased by 30% with increasing distance from the heart (equivalent to positions *1int* to *6int*). Zou and Zhang (2009) reported the same trend in bovine thoracic aorta. Those studies did not include the abdominal aorta. In the mouse thoracic there was a slight (6%) increase in elastic modulus from *1int* to *6int* in the purified elastin ring when the lamellar stress was used (see Figure 16 b) but not in the intact or when engineering stress was used. The regional variation in elastic modulus may be different between these two species (although pig abdominal aorta data is lacking), however three studies (the current study; Lillie and Gosline, 2007; Zou and Zhang, 2009) have now found that the elastic modulus of elastin does change with longitudinal position along the aorta.

Morphology

The second part of this thesis attempted to determine what causes the elastic modulus of the purified elastin mouse abdominal aorta to be 43% lower than the thoracic aorta by investigating the morphology of elastin in the aortic wall. The elastic modulus was compared at six positions along the mouse aorta; the morphological portion of this thesis focuses on one area of the thoracic and one area of the abdominal aorta (roughly equivalent to the *6int* and *ilia* positions).

Hypotheses

Six hypotheses were put forward to describe the mechanism for the decrease in elastic modulus in the abdominal aorta and five hypotheses were tested in this study. The five hypotheses relate to the structure of elastin in the aortic media and its partitioning among the three forms: elastic lamellae, interlamellar elastin fibres (IEF) and elastin struts.

Hypothesis One: Amount of Elastin

The first hypothesis was that there was a difference in the amount of elastin in the thoracic and abdominal aortas. Normalizing the data should account for the amount of elastin in the sample and remove any trends that a difference would cause but the data were examined to confirm that no artefacts were introduced when normalizing the data.

The volume fraction of elastin was 33% lower in the abdominal aorta than the thoracic (see Figure 23 b) which is largely accounted for by the 44% increase in the lamellar unit thickness in the abdominal aorta (see Figure 23 a) but does not necessarily reflect the amount of elastin. When the amount of elastin is accounted for by normalizing the data by the number of elastic lamellae and thickness of the lamellae (lamellar stress) the trend remains (see Figure 16 b). If the trend in modulus was caused by a decrease in the amount of elastin in the abdominal aorta, normalizing the data would have eliminated the trend.

However, the fibre packing density of elastin in the elastic lamellae must also be considered because it would affect the elastic modulus. Unfortunately the fibre packing density could not be measured with the MPSLM data obtained during this study. Lillie and Gosline (2007) accounted for the fibre packing density of elastin in pig thoracic aorta rings and although it accounted for some of the change in elastic modulus along the aorta, it did not account for all of it. Until the elastin fibre packing density is measured in the mouse aorta, this hypothesis cannot be rejected.

Hypothesis Two: Interlamellar Elastin Fibres (IEF)

The second hypothesis was that the decrease in elastic modulus in the abdominal aorta was due to the amount of IEF or their orientation. The IEF protrude obliquely from the elastic lamellae and attach to smooth muscle cells (Davis, 1993; O'Connell et al., 2008). Other IEF connect those smooth muscle cells to the next elastic lamella in the same orientation, providing a connection from one elastic lamella to the next via the smooth muscle cells. Since the IEF run in the oblique orientation they will contribute to the circumferential elastic stiffness of the aorta wall. Therefore a difference in their number or orientation between the thoracic and abdominal aortas could cause a change in elastic modulus.

I tested this hypothesis by autoclaving the tissue to remove the smooth muscle cells and therefore break the IEF connections, rendering them mechanically inactive. The elastic modulus of intact aorta rings will therefore include the contribution of IEF whereas the elastic modulus of purified elastin aorta rings will not. If the decrease in elastic modulus in the abdominal aorta was caused by the IEF, I would expect to see the trend disappear (constant elastic modulus) in the purified elastin data. Figure 16 (a) is reproduced below with lines of best fit to emphasize the trend (see Figure 24). The modulus did drop on autoclaving so the IEF might provide about 19% of the elastin resistance to deformation in the thoracic aorta and 20% in the abdominal. This is different than in previous studies in pigs [26% for the carotid artery; (Roy et al., 2008) and no difference in the thoracic aorta; (Lillie et al., 2012)] However, since the same trend in elastic

modulus is seen in intact and purified elastin data, the decrease in stiffness in the abdominal aorta could not be caused by the IEF and so this hypothesis was rejected.

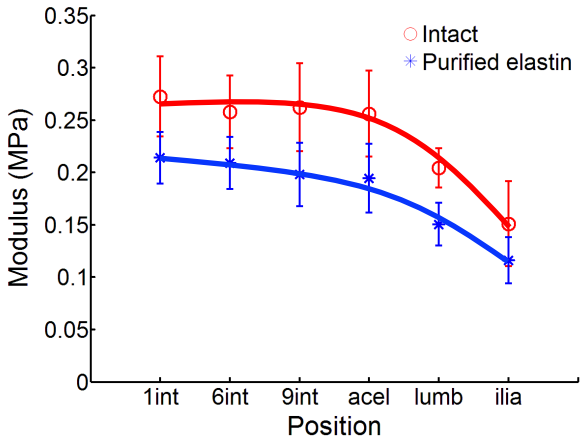

Figure 24. Elastic modulus of mouse aorta rings at six positions along the aorta, three in the thoracic (*1int*, *6int*, *9int*) and three in the abdominal (*acel*, *lumb*, *ilia*). Red circles are intact rings (before autoclaving) and blue stars are purified elastin rings (after autoclaving). Stress is from engineering stress; stretch ratio is from regression initial length. Lines of best fit are shown to emphasize the similar trend in the data. Means ± 95% CI. n = 9 for all intact rings. For purified elastin rings, n = 9 (*9int* and *lumb*), n = 8 (*6int*, *acel* and *ilia*), and n = 7 (*1int*).

Hypothesis Three: Partitioning of Elastin

The third hypothesis was that the partitioning of the elastin between lamellar elastin (elastic lamellae) and interlamellar elastin (IEF and struts) might be different in the thoracic and abdominal aortas. To test this hypothesis the surface area of elastin was compared in the thoracic and abdominal aortas as a greater amount of interlamellar elastin (which contains smaller structures than lamellar elastin) might increase the surface area of elastin. There was no difference in the surface area of elastin in the thoracic and abdominal aortas when normalized by either the volume fraction of elastin or the number of elastic lamellae (see Figure 23 e and f) and so this hypothesis was rejected.

Hypothesis Four: Elastic Lamellae Thickness or Orientation

The fourth hypothesis was that the elastic lamellae thickness or orientation could be different in the thoracic and abdominal aortas, causing a difference in elastic modulus. As with the amount of elastin (above), elastic lamellae thickness should be accounted for in normalizing the data (see Equation 4), but the values were compared as a confirmation. There was no

significant difference in the thickness of the elastic lamellae so this part of the hypothesis was rejected (see Figure 23 c).

The fibres that make up the elastic lamellae are reported by some to be oriented circumferentially in the aortic media (O'Connell et al., 2008) making a direct contribution to the circumferential elastic modulus. Others report that the elastic lamellae are oriented at some angle not directly circumferential (Hollander et al., 2011). If the elastic lamellae fibres were oriented slightly helically in the abdominal aorta, the circumferential elastic modulus might be decreased. Examination of the elastic lamellae in both the thoracic and abdominal aortas confirms the circumferential orientation and so this hypothesis was also rejected (see Figure 20 a, b, c).

Hypothesis Five: Struts

The fifth and last hypothesis was that the number of struts could differ in the thoracic and abdominal aortas. The struts appear to be oriented radially, connecting one elastic lamella to the next (see Figure 20 h and Figure 21), which is what has been reported previously (O'Connell et al., 2008). It isn't clear how the struts would contribute to the circumferential modulus because of their radial orientation but the aortic media is a complex structure and nature may have found a way.

It has been observed that the aortic wall of a purified elastin aorta deforms at a constant volume (Lillie et al., 2010). In other words, it doesn't collapse even though the smooth muscle cells and collagen have been removed by autoclaving and there is no longer anything between the elastic lamellae holding them apart. Perhaps it is the struts that hold the elastic lamellae apart and this somehow contributes to the circumferential elastic modulus.

Unfortunately it wasn't possible to count the struts from the MPLSM images to test this hypothesis. In some areas the struts were easy to count but in others there were so many that it was impossible (see Figure 21). Where the elastic lamellae are close together it appears that

there are many struts but this could also be an artefact created when rendering the 3D model. The Amira software assumes that data points that are close together are connected, so areas where the elastic lamellae are very close together may appear full of struts when they are not.

The struts in the thoracic and abdominal aortas must be quantified to fully address this hypothesis but the current protocol did not allow it. Therefore the strut hypothesis cannot be rejected.

MPLSM Limitations

The MPLSM used in this study had some limitations when used with this type of tissue but none of these limitations are thought to have affected the results reported here.

The IEF are thin (approximately 0.5 μm diameter; O'Connell et al., 2008) and oriented in almost the same plane as the laser beam during the scan, so they may not have been picked up in the signal. Their contribution to the elastic modulus was ruled out using mechanical testing data so not having them in the MPLSM data was not a hindrance.

Some other materials like lipids also fluoresce and were also picked up in the signal with the elastin. The aorta wall is not permeable and so it is assumed that any elastin signal coming from the interior of the wall is in fact elastin, as no other substances could enter into the media.

Some samples had areas where fluorescence was not detected, leaving a hole in the data. Due to the non-uniform nature of these holes, they were assumed to be artefacts. These missing data would affect the volume of elastin and contribute to some of the variation seen in the volume data.

Future Direction

The fibre packing density of the elastic lamellae was not addressed in this study so the next step would be to compare the fibre packing density of the elastic lamellae in the thoracic

and abdominal aortas. This could be done with the same MPLSM technique with the focus shifted to the elastic lamellae instead of the entire media, or with electron microscopy.

This thesis was not able to address the hypothesis that a difference in the number of struts between the thoracic and abdominal aortas could cause a change in elastic modulus. In the future another method could be used to quantify the struts, for example electron microscopy. Electron microscopy has been used to answer other questions regarding the structure of the aorta wall (O'Connell et al., 2008) and could therefore be a suitable tool to quantify struts.

Another hypothesis that this thesis has not examined is the possibility that the elastin could have a different cross-linking density along the aorta, leading to a different elastic modulus. Cross-linking density has not been examined in the elastin of the aorta wall; however, alternate splicing (Sugitani et al., 2012) in the elastin gene could affect the elastin cross-linking density in the thoracic and abdominal aortas.

As well as further studies into the mechanism for the change in elastic modulus along the aorta, it would also be valuable to know how widespread this phenomenon is in other species. The original study carried out on pig thoracic aortas could be expanded to include abdominal aortas, filling in that data set. The aortic media of all mammals has similar mechanical properties (Wolinsky and Glagov, 1967) so expanding the study to non-mammalian species could shed light on the mechanical properties of elastin in the aortic wall through the similarities and differences found among species.

Conclusions

This thesis provides strong data from tensile tests showing that there is a decrease in elastic modulus of the elastin in the abdominal aorta compared with the thoracic. Many possible explanations for this have been ruled out with two hypotheses remaining: that the decrease in elastic modulus is due to some difference in the interlamellar elastin struts between the thoracic

and abdominal aortas or due to a difference in the fibre packing density of the elastic lamellae. Further studies with the goal of quantifying the struts in the aortic media and measuring the fibre packing density of the elastic lamellae are required to address these hypotheses.

The structure and mechanical properties of the aorta wall change along its length, as does the loading of the wall due to pressure wave reflections. Much of this variation is due to the changing proportions of elastin and collagen along the length of the aorta; however, it is becoming apparent that the mechanical properties of elastin also vary along the aorta. It is critical to identify how and why this variation occurs in order to understand artery physiology and pathologies, and also to provide the data for modelling healthy and diseased aortas.

References

Aaron, B. B. and Gosline, J. M. (1981). Elastin as a random-network elastomer: a mechanical and optical analysis of single elastin fibres. *Biopolymers* **20,** 1247.

Aaron, B. B. and Gosline, J. M. (1980). Optical properties of single elastin fibres indicate random protein conformation. *Nature* **287,** 865-867.

Attinger, E. O. (1964). Elements of theoretical hydrodynamics. In *Pulsatile blood flow* (ed. E. O. Attinger). New York: McGraw-Hill.

Bergel, D. H. (1960). The visco-elastic properties of the arterial wall.

Boedtker, H. and Doty, P. (1956). The Native and Denatured States of Soluble Collagen. *J. Am. Chem. Soc.* **78,** 4267.

Clark, J. and Glagov, S. (1985). Transmural organization of the arterial media. The lamellar unit revisited. *Arterioscl. Thromb. Vas.* **5,** 19-34.

Cox, R. H. (1983). Comparison of arterial wall mechanics using ring and cylindrical segments. *Am. J. Physiol. - Heart C.* **244,** H298-H303.

Davis, E. C. (1993). Smooth muscle cell to elastic lamina connections in developing mouse aorta. Role in aortic medial organization. *Lab. Invest.* **68,** 89-99.

Dingemans, K. P., Teeling, P., Lagendijk, J. H. and Becker, A. E. (2000). Extracellular matrix of the human aortic media: an ultrastructural histochemical and immunohistochemical study of the adult aortic media. *Anat. Rec.* **258,** 1-14.

Dobrin, P. and Canfield, T. (1977). Identification of smooth muscle series elastic component in intact carotid artery. *Am. J. Physiol. - Heart C.* **232,** H122-H130.

Fischer, G. M. and Llaurado, J. G. (1966). Collagen and elastin content in canine arteries selected from functionally different vascular beds. *Circ. Res.* **19,** 394-399.

Fung, Y. (1993). *Biomechanics: mechanical properties of living tissues*. New York: Springer-Verlag.

Gundiah, N., B Ratcliffe, M. and A Pruitt, L. (2007). Determination of strain energy function for arterial elastin: Experiments using histology and mechanical tests. *J. Biomech.* **40,** 586-594.

Guo, X., Kono, Y., Mattrey, R. and Kassab, G. S. (2002). Morphometry and strain distribution of the C57BL/6 mouse aorta. *Am. J. Physiol. - Heart C.* **283,** H1829-H1837.

Guo, X. and Kassab, G. S. (2003). Variation of mechanical properties along the length of the aorta in C57bl/6 mice. *Am. J. Physiol. - Heart C.* **285,** H2614-H2622.

Hales, S. (1733). *Statistical essays: Containing haemastatics*. London.

Harkness, M. L. R., Harkness, R. D. and McDonald, D. A. (1957). The collagen and elastin content of the arterial wall in the dog. *P. Roy. Soc. Lond. B Bio.***146,** 541-551.

Harvey, W. (1628). *The circulation of the blood and other writings*. New York: Dutton.

Hollander, Y., Durban, D., Lu, X., Kassab, G. and Lanir, Y. (2011). Experimentally validated microstructural 3D constitutive model of coronary arterial media. *J. Biomech. Eng.* **133**.

Huang, Y., Guo, X. and Kassab, G. S. (2006). Axial nonuniformity of geometric and mechanical properties of mouse aorta is increased during postnatal growth. *Am. J. Physiol. - Heart C.* **290,** H657-H664.

Ker, R. F. (1981). Dynamic tensile properties of the plantaris tendon of sheep (Ovis aries). *J. Exp. Biol.* **93,** 283-302.

Lillie, M. A., Chalmers, G. W. G. and Gosline, J. M. (1994). The effects of heating on the mechanical properties of arterial elastin. *Connect. Tiss. Res.* **31,** 23-35.

Lillie, M. A., Armstrong, T. E., Gérard, S. G., Shadwick, R. E. and Gosline, J. M. (2012). Contribution of elastin and collagen to the inflation response of the pig thoracic aorta: Assessing elastin's role in mechanical homeostasis. *J. Biomech.* **45,** 2133-2141.

Lillie, M. A., David, G. J. and Gosline, J. M. (1998). Mechanical Role of Elastin-Associated Microfibrils in Pig Aortic Elastic Tissue. *Connect. Tiss. Res.* **37,** 121-141.

Lillie, M. A. and Gosline, J. M. (2007). Mechanical properties of elastin along the thoracic aorta in the pig. *J. Biomech.* **40,** 2214-2221.

Lillie, M. A., Shadwick, R. E. and Gosline, J. M. (2010). Mechanical anisotropy of inflated elastic tissue from the pig aorta. *J. Biomech.* **43,** 2070-2078.

Megens, R. T. A., Reitsma, S., Schiffers, P. H. M., Hilgers, R. H. P., De Mey, J. G. R., Slaaf, D. W., oude Egbrink, M. G. A. and van Zandvoort, M. A. M. J. (2007). Two-photon microscopy of vital murine elastic and muscular arteries. Combined structural and functional imaging with subcellular resolution. *J. Vasc. Res.* **44,** 87-98.

National Institutes of Health. ImageJ 1.46r.

O'Connell, M. K., Murthy, S., Phan, S., Xu, C., Buchanan, J., Spilker, R., Dalman, R. L., Zarins, C. K., Denk, W. and Taylor, C. A. (2008). The three-dimensional micro- and nanostructure of the aortic medial lamellar unit measured using 3D confocal and electron microscopy imaging. *Matrix Biol.* **27,** 171-181.

Partridge, S. M., Davis, H. F. and Adair, G. S. (1955). The chemistry of connective tissues. 2. Soluble proteins derived from partial hydrolysis of elastin. *Biochem. J.* **61,** 11-21.

Roach, M. R. and Burton, A. C. (1957). The reason for the shape of the distensibility curves of arteries. *Can. J. Biochem. Physiol.* **35,** 681-690.

Roy, S., Tsamis, A., Prod'hom, G. and Stergiopulos, N. (2008). On the in-series and in-parallel contribution of elastin assessed by a structure-based biomechanical model of the arterial wall. *J. Biomech.* **41,** 737-743.

Shadwick, R. E. (1999). Mechanical design in arteries. *J. Exp. Biol.* **202,** 3305-3313.

Shadwick, R. E. (1998). Elasticity in arteries: a similar combination of rubbery and stiff materials creates common mechanical properties in blood vessels of vertebrates and some invertebrates. *Am. Sci.* **86,** pp. 535-541.

Song, S. H. and Roach, M. R. (1985). A morphological comparison of aortic elastin from five species as seen with the scanning electron microscope. *Acta. Anat.* **123,** 45-50.

Sugitani, H., Hirano, E., Knutsen, R.H., Shifren, A., Wagenseil, J.E., Ciliberto, C., Kozel, B.A., Urban, Z., Davis, E.C., Broekelmann, T.J. and Mecham, R.P. (2012). Alternative splicing and tissue-specific elastin misassembly act as biological modifiers of human elastin gene frameshift mutations associated with dominant cutis laxa. *J. Biol. Chem.* **287,** pp. 22055-22067.

Taylor, M. G. (1964). Wave travel in arteries and the design of the cardiovascular system. In *Pulsatile blood flow* (ed. E. O. Attinger), pp. 343-372. New York: McGraw-Hill.

Wolinsky, H. and Glagov, S. (1964). Structural basis for the static mechanical properties of the aortic media. *Circ. Res.* **14,** 400-413.

Wolinsky, H. and Glagov, S. (1967). A lamellar unit of aortic medial structure and function in mammals. *Circ. Res.* **20,** 99-111.

Zipfel, W. R., Williams, R. M. and Webb, W. W. (2003). Nonlinear magic: multiphoton microscopy in the biosciences. *Nat. Biotechnol.* **21,** 1369-1377.

Zou, Y. and Zhang, Y. (2009). An experimental and theoretical study on the anisotropy of elastin network. *Ann. Biomed. Eng.* **37,** 1572-1583.

Appendix – Experimental Data

Mouse	Intact			Purified Elastin (4 hr)		
	Thoracic Modulus (*6int*) (MPa)	Abdominal Modulus (*ilia*) (MPa)	% Difference	Thoracic Modulus (*6int*) (MPa)	Abdominal Modulus (*ilia*) (MPa)	% Difference
AB	---	0.08	---	---	0.06	---
AC	0.22	0.16	0.27	0.16	0.10	0.36
AD	0.20	0.09	0.56	0.16	0.09	0.46
AE	0.37	0.28	0.24	0.26	0.16	0.40
AF	0.26	0.19	0.29	0.22	0.15	0.35
AG	0.25	0.13	0.48	0.24	0.12	0.51
AH	0.28	0.14	0.50	0.21	0.11	0.48
AI	0.27	---	---	0.23	---	---
AK	0.22	0.14	0.35	0.19	0.15	0.22
Mean	**0.26 ± 0.03**	**0.15 ± 0.04**	**0.42**	**0.21 ± 0.02**	**0.12 ± 0.02**	**0.43**

Table A-6. Moduli of mouse thoracic and abdominal aorta rings. Stress from engineering stress; stretch ratio from regression initial length.

Mouse	Intact			Purified Elastin (4 hr)		
	Thoracic Modulus (*6int*) (MPa)	Abdominal Modulus (*ilia*) (MPa)	% Difference	Thoracic Modulus (*6int*) (MPa)	Abdominal Modulus (*ilia*) (MPa)	% Difference
AB	---	0.61	---	---	0.44	---
AC	1.00	0.72	0.28	0.73	0.46	0.37
AD	1.02	0.50	0.51	0.80	0.49	0.39
AE	1.06	0.79	0.25	0.75	0.45	0.40
AF	0.86	0.61	0.29	0.72	0.47	0.35
AG	0.78	0.62	0.20	0.75	0.57	0.24
AH	0.89	0.52	0.42	0.67	0.40	0.40
AI	0.78	---	---	0.66	---	---
AK	0.64	0.46	0.28	0.57	0.49	0.14
Mean	**0.88 ± 0.09**	**0.60 ± 0.07**	**0.32**	**0.71 ± 0.05**	**0.47 ± 0.03**	**0.34**

Table A-7. Moduli of mouse thoracic and abdominal aorta rings. Stress from lamellar stress; stretch ratio from regression initial length.

Mouse	Intact			Purified Elastin (4 hr)		
	Thoracic Modulus (*6int*) (MPa)	Abdominal Modulus (*ilia*) (MPa)	% Difference	Thoracic Modulus (*6int*) (MPa)	Abdominal Modulus (*ilia*) (MPa)	% Difference
AB	---	0.06	---	---	0.44	---
AC	0.16	0.18	-0.08	0.12	0.11	0.08
AD	0.15	0.09	0.41	0.13	0.09	0.36
AE	0.23	0.24	-0.06	0.20	0.15	0.23
AF	0.20	0.16	0.21	0.17	0.14	0.20
AG	0.20	0.10	0.51	0.20	0.10	0.49
AH	0.21	0.13	0.37	0.17	0.12	0.31
AI	0.23	---	---	0.19	---	---
AK	0.19	0.13	0.32	0.17	0.13	0.22
Mean	**0.20 ± 0.02**	**0.14 ± 0.04**	**0.30**	**0.17 ± 0.02**	**0.11 ± 0.02**	**0.35**

Table A-8. Moduli of mouse thoracic and abdominal aorta rings. Stress from engineering stress; stretch ratio from morphological initial length.

Mouse	Intact			Purified Elastin (4 hr)		
	Thoracic Modulus (*6int*) (MPa)	Abdominal Modulus (*ilia*) (MPa)	% Difference	Thoracic Modulus (*6int*) (MPa)	Abdominal Modulus (*ilia*) (MPa)	% Difference
AB	---	0.06	---	---	0.05	---
AC	0.19	0.15	0.23	0.14	0.09	0.32
AD	0.16	0.05	0.68	0.14	0.07	0.47
AE	0.32	0.24	0.23	0.23	0.14	0.36
AF	0.23	0.14	0.38	0.20	0.13	0.33
AG	0.21	0.10	0.52	0.21	0.11	0.49
AH	0.24	0.11	0.52	0.19	0.11	0.44
AI	0.24	---	---	0.20	---	---
AK	0.25	0.13	0.49	0.20	0.14	0.29
Mean	**0.23 ± 0.03**	**0.12 ± 0.04**	**0.48**	**0.19 ± 0.02**	**0.11 ± 0.02**	**0.42**

Table A-9. Moduli of mouse thoracic and abdominal aorta rings. Stress from engineering stress; stretch ratio from mechanical initial length.

Mouse	Circumferential Stretch Ratio		Longitudinal Stretch Ratio	
	Thoracic	Abdominal	Thoracic	Abdominal
MC	1.41	1.11	---	1.13
MG	1.27	1.05	1.51	1.02
MH	1.21	1.17	1.07	1.04
MI	1.20	1.55	1.08	1.12
MJ	1.23	1.04	1.10	1.09
MK	1.23	1.13	1.17	---
ML	1.61	---	---	---
MM	1.38	1.39	---	1.10
Mean	**1.32 ± 0.10**	**1.21 ± 0.14**	**1.11 ± 0.04**	**1.08 ± 0.03**

Table A-10. Circumferential and longitudinal stretch ratios of mouse aortas.

Mouse	Deformed (uncorrected)			Undeformed (corrected)			Number of Elastic Lamellae
	Media Thickness (µm)	Elastic Lamellae Thickness (µm)	Lamellar Unit Thickness (µm)	Media Thickness (µm)	Elastic Lamellae Thickness (µm)	Lamellar Unit Thickness (µm)	
MC	34.48	1.91	7.11	50.19	2.77	10.35	5.75
MG	23.85	1.68	7.42	34.73	2.44	10.80	5
MH	24.70	1.42	5.24	35.96	2.06	7.63	6
MI	31.94	2.13	6.36	46.50	3.11	9.26	5.5
MJ	28.64	1.82	5.45	41.70	2.66	7.94	6
MK	37.43	2.09	7.73	54.50	3.05	11.26	5.75
ML	16.94	2.01	4.86	24.66	2.93	7.07	5
MM	22.96	1.82	4.37	33.43	2.65	6.36	6
Mean	**27.62**	**1.86**	**6.07**	**40.21**	**2.71**	**8.83**	**5.6**

Table A-11. Thoracic aorta media thickness, elastic lamellae thickness, and lamellar unit thickness. Values are shown for the deformed (pressurized) state and the undeformed (no pressure) state after the correction factor.

Mouse	Deformed (uncorrected)			Undeformed (corrected)			Number of Elastic Lamellae
	Media Thickness (µm)	Elastic Lamellae Thickness (µm)	Lamellar Unit Thickness (µm)	Media Thickness (µm)	Elastic Lamellae Thickness (µm)	Lamellar Unit Thickness (µm)	
MC	31.23	2.11	10.5	40.77	2.76	13.71	4
MG	46.79	2.19	15.8	61.10	2.85	20.63	4
MH	20.16	1.38	7.3	26.32	1.81	9.53	4.25
MI	24.84	2.80	7.61	32.44	3.66	9.94	4
MJ	21.15	1.92	6.68	27.61	2.50	8.72	4
MK	28.14	1.89	10.40	36.75	2.46	13.58	3.75
ML	29.36	2.25	11.28	38.34	2.93	14.72	4
MM	28.48	2.47	8.17	37.19	3.23	10.67	4.25
Mean	**28.77**	**2.13**	**9.72**	**37.57**	**2.77**	**12.69**	**4.0**

Table A-12. Abdominal aorta media thickness, elastic lamellae thickness, and lamellar unit thickness. Values are shown for the deformed (pressurized) state and the undeformed (no pressure) state after the correction factor.

Mouse	% Elastin Volume in Sample Volume	Surface Area / # Elastic Lamellae (μm^2)	Surface Area / Elastin Volume (μm^{-1})
MC	0.46	80079	0.89
MG	0.34	50203	1.04
MH	0.39	60060	1.14
MI	0.34	86848	1.41
MJ	0.38	77564	1.28
MK	0.56	75914	0.62
ML	0.53	49529	0.99
MM	0.58	61713	0.80
Mean	**0.45**	**67739**	**1.02**

Table A-13. Thoracic aorta elastin volume as a percentage of the sample volume, surface area normalized by the number of elastic lamellae and surface area normalized by elastin volume.

Mouse	% Elastin Volume in Sample Volume	Surface Area / # Elastic Lamellae (μm^2)	Surface Area / Elastin Volume (μm^{-1})
MC	0.24	73673	1.36
MG	0.14	53847	1.12
MH	0.28	49633	2.33
MI	0.23	81754	1.93
MJ	0.37	77669	1.26
MK	0.32	74735	1.10
ML	0.31	94550	1.02
MM	0.51	90231	0.81
Mean	**0.30**	**74512**	**1.37**

Table A-14. Abdominal aorta elastin volume as a percentage of the sample volume, surface area normalized by the number of elastic lamellae and surface area normalized by elastin volume.